An Investigation into Methods for Electrospinning Poly(ether ether ketone)

Thomas R. Keller

Tufts University

An Undergraduate Honors Thesis submitted for the degree of

Bachelor of Science

May 20, 2018

With thesis Advisor

Professor Peggy Cebe

Table of Contents

List of Figures 4

List of Tables 5

Acknowledgements 6

Abstract 7

Chapter 1 – Introduction

1.1 – Background 8

1.2 - Introduction to Polymers and PEEK 8

1.3 – Electrospinning 12

1.4 – Electrospun Fibers and Applications 15

1.5 - Electrospinning PEEK 17

1.6 - Validating Results 18

Chapter 1 References 20

Chapter 2 – Experiment 21

2.1 – Polymer Choice 22

2.2 –Temperature 23

2.3 – Electric Field 25

2.4 – Spinneret 26

2.5 – Collector 30

2.6 - Working Distance 32

2.7 – Full Experimental Method 35

Chapter 2 References 41

Chapter 3 – Results

3.1 – Overview 42

3.2 – SEM Results 42

3.2.1 – Fiber Orientation 42

3.2.2 – Fiber Diameters 49

3.2.3 – Unique Characteristics 56

3.3 – TGA Results 63

3.4 – FTIR Results 66

3.5 – POM Results 73

Chapter 3 References 77

Chapter 4 – Conclusions and Future Work

4.1 – Experimental Limitations…… 79

4.2 – Fiber Quality…… 83

4.3 – Application Potential…… 83

4.4 - Future Work…… 84

Chapter 4 References…… 86

List of Figures

Chapter 1:

Figure 1.1 – The chemical structure of PEEK

Figure 1.2 – The chemical process of PEEK sulfonation

Figure 1.3 – Taylor cone formation

Figure 1.4 – A typical melt electrospinning setup

Figure 1.5 – A direct writing melt electrospinning setup

Chapter 2:

Figure 2.1 – Resistive heating spinneret

Figure 2.2 – Thermolyne 2000 furnace calibration

Figure 2.3 – Wiring layout within furnace and spinneret wire

Figure 2.4 – Tungsten wire basket

Figure 2.5 – Tungsten basket as spinneret in furnace

Figure 2.6 – PEEK droplet Taylor cones

Figure 2.7 – Aluminum foil collector

Figure 2.8 – Collector mounted on insulating stand

Figure 2.9 – Empty furnace

Figure 2.10 – Measuring working distance

Figure 2.11 – Measuring spinneret temperature

Figure 2.12 – Front view of furnace without collector

Figure 2.13 – DC power supply

Figure 2.14 – PEEK fibers on a collector

Chapter 3:

Figures 3.1 to 3.11 – SEM Images of fiber samples 1 to 11

Figure 3.12 – SEM image of sample 9

Figure 3.13 – SEM image of very small fibers among large fibers

Figure 3.14 – SEM image of solution electrospun beads

Figure 3.15 – Optical image of PEEK fiber looping

Figure 3.16 – Effect of surface speed on fiber looping

Figure 3.17 – SEM image of spherulites on fiber surface

Figure 3.18 – SEM image side view of fiber mound

Figure 3.19 – Spin line profile of melt electrospun polypropylene

Figure 3.20 – TGA curve of PEEK fiber droplet

Figure 3.21 – TGA curve of PEEK pellet

Figure 3.22 – TGA curve of S-PEEK

Figure 3.23 – FTIR spectra of PEEK pellet and fibers

Figure 3.24 – FTIR spectra of PEEK and S-PEEK from1800 to 1350 cm^{-1}

Figure 3.25 – FTIR spectra of PEEK and S-PEEK from 1350 to 900 cm^{-1}

Figure 3.26 – FTIR spectra of PEEK and S-PEEK from 900 to 650 cm^{-1}

Figure 3.27 – POM images of birefringent fiber

Chapter 4:

Figure 4.1 – Diagram of a potential extruder and spinneret design

Figure 4.2 – PEEK fiber distribution on the collector

Figure 4.3 – Branching and whipping of solution electrospinning

List of Tables

Chapter 1:

Table 1.1 – Physical, thermal, and electrical properties of PEEK

Table 1.2 – Chemical resistance of PEEK

Chapter 2:

Table 2.1 – Comparison of different grades of PEEK

Table 2.2 – Comparison of similar melt electrospun polymers

Chapter 3:

Table 3.1 – Histograms of fiber diameters at various electric field strengths

Table 3.2 – Characterisitic FTIR spectra for PEEK

Acknowledgements

First and foremost, I want to thank Prof. Peggy Cebe for her outstanding advice, guidance, and patience through the course of this thesis. Her example as a scientist and an expert in her field gave me the confidence to undertake this difficult challenge.

Second, I want to thank the wonderful members of the Cebe Research Group at Tufts University. Dave Thomas, Nelaka Govinna, Andrew Clark, and many others were always there to help me develop new ideas and to lend a helping hand when I needed it.

Third, I want to thank Prof. Hugh Gallagher, the Tufts Physics Department, and the University as a whole. The resources and support afforded to me as an undergraduate researcher were of the highest standard, and I cannot imagine undertaking this thesis at any other institution.

Fourth, I want to thank the National Science Foundation for its funding and ongoing support of scientists all over this country.

Finally, to my friends, my family, and everyone who helped me through this year of trial and triumph: thank you.

Abstract

Electrospinning is a well-established method for forming polymers into micron and sub-micron size fibers. During electrospinning a polymer in a liquid state, either in solution or molten, is drawn into a fibrous shape using applied high voltage. This thesis sets out to show a new method for electrospinning Poly(ether ether ketone) (PEEK). PEEK has thermal, chemical, and mechanical properties that make it desirable for many applications in filtration and textiles. However, these desirable properties also make PEEK a difficult material to process. It is insoluble in most common solvents at room temperature, with the exception of Sulfuric Acid at greater than 95% concentration. Yet, PEEK undergoes a reaction known as sulfonation when dissolved in Sulfuric Acid. Sulfonation adversely affects PEEK's thermal and chemical properties. Therefore, this thesis provides a method for electrospinning PEEK without sulfonation, by electrospinning the polymer in a molten state rather than in solution. By keeping PEEK in its native, unsulfonated state, the resulting fibers are shown to retain their thermal and chemical properties. Furthermore, the fibers are shown to be of micron and sub-micron size. To the best of my knowledge, this thesis presents the first successful method for electrospinning native PEEK fibers.

Chapter 1 - Introduction

1.1 – Background

Poly(ether ether ketone) (PEEK) is a high-performance semicrystalline thermoplastic polymer. First commercialized by Imperial Chemical Industries PLC (ICI) in 1978, PEEK has been employed in a number of diverse applications due to its unique thermal, mechanical, and chemical properties [1]. As a thermoplastic, PEEK can be heated past its melting point into a liquid and then cooled back to a solid state, allowing it to be manufactured into molded parts, seals, films, and fibers [2]. The purpose of this research thesis is to investigate the possibility of forming elongated PEEK fibers using the melt electrospinning method. Related research into electrospinning similar polymers has yielded fibers of single micron diameters. Investigating methods of electrospinning PEEK is critical for understanding its potential applications in micro-scale fiber technologies such as filtration and textiles [3].

1.2 – Introduction to Polymers and PEEK

Polymers are large, complex molecules made up of simpler repeating units called monomers. Polymers can be found in all sorts of everyday products, ranging from synthetic fabrics for clothing, rubber for shoes and tires, and the rigid plastics found in consumer and industrial goods. A polymer's properties are closely linked to its formative repeating units as well as the structural way these units are organized [4]. Due to its internal organization of repeating phenyl groups, PEEK falls into the engineering polymer family of Poly(aryl ether ketone)s or PAEKs. In PEEK's backbone, the longest series of covalently bonded atoms in the molecule, there are two ether and one ketone group (see Figure 1.1).

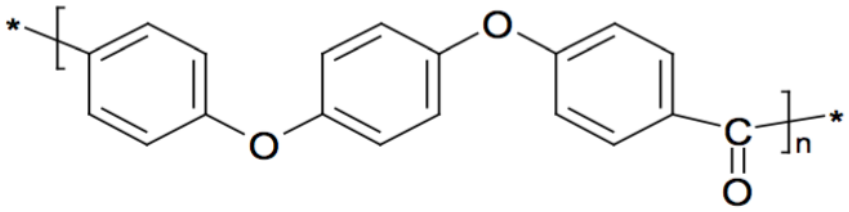

Figure 1.1: The chemical structure of PEEK. Note the ether groups containing a single bond oxygen atom and the ketone group containing a double bond oxygen atom. The hexagonal shapes represent the three aromatic (aryl) phenyl rings [1] (image from [5]).

Relative to other polymers, PEEK has a high tensile strength of 105 MPa, a high melting and degradation point of 343 °C and 595 °C respectively [5], and is chemically resistant to most common solvents at room temperature with only a few exceptions (see Table 1.1 and 1.2).

Table 1.1: A basic summary of physical, thermal, and electrical properties of PEEK

Property	Value*	Units
Tensile Elongation	30	% At Break
Tensile Modulus	4.1	GPa
Flexural Modulus	3.9	GPa
Charpy Impact Strength	4.2	kJm^{-2} Notched
Compressive Strength	130	MPa
Glass Transition Onset	143	Degrees C
Melting Point	343	Degrees C
Dielectric Strength	23	kV/mm at 2mm thickness

*(Victrex 150/151G) [2].

Table 1.2: A summary of the chemical resistance of PEEK at different temperatures.

Solvent	20°C	60°C	100°C
Acetone	R*	R	R
Alcohols	R	R	R
Bromine	NR	NR	NR
Chloroform	R	R	R
Formic Acid	R	R	R
Hydrochloric Acid	R	R	ND
Hydrogen Peroxide (30%)	R	R	R
Methanol	R	R	R
Nitric Acid (50%)	R	R	R
Perchloric Acid	R	R	R
Sulfuric Acid (70%)	R	R	R
Sulfuric Acid (95%)	NR	NR	NR

* R stands for resistant, NR for not resistant, and ND for no data [1].

These properties make PEEK a desirable engineering material, but also make it difficult to process. Despite the challenges, the unique characteristics of PEEK, specifically its thermal and chemical resilience, have garnered interest in developing its potential as a micro-porous filtration membrane. Research in this area has shown that porous PEEK membranes can be formed from a solution of PEEK in certain sulfuric and sulfonic acids. This solution is cast into a thin film and the solvent is evaporated leaving a porous membrane [6]. However, the downside to this method is that PEEK usually becomes sulfonated in this process and gains a side chain molecule, changing from unsulfonated "native" PEEK to S-PEEK (see Figure 1.2). The addition of this molecule lessens some of PEEK's desirable characteristics, including lowering the degradation temperature, at which

significant mass loss occurs, to at most 530°C and as low as 345°C depending on the counter-ion present [7]. S-PEEK does however show many characteristics that make it desirable in fuel cell membrane applications, including good proton conductivity [6,8].

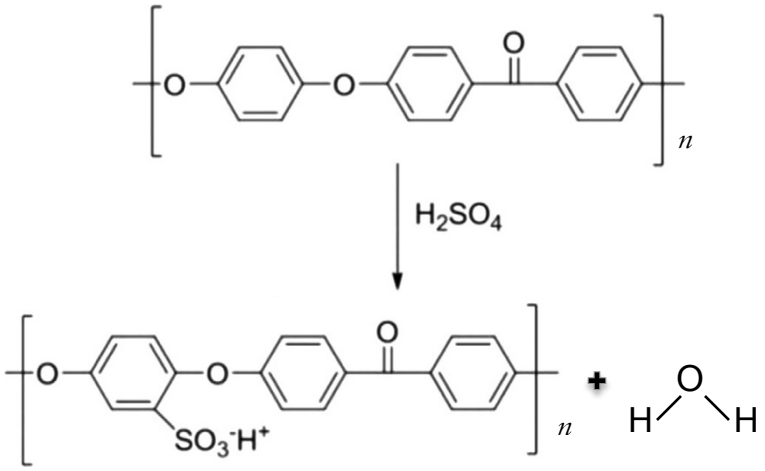

Figure 1.2: The chemical process by which PEEK becomes sulfonated in sulfuric acid (image from [9]). This reaction produces sulfonated PEEK as well as H_2O.

Alternate research has been done to form a porous PEEK membrane using Thermally Induced Phase Separation (TIPS). In this case, the PEEK is combined with a diluent at a temperature where both are in a liquid state. Upon cooling, phase separation occurs and the diluent can be selectively removed using a solvent, leaving behind porous vacancies in the PEEK structure [1,10]. da Silva Burgal, *et al.* [9] report the production of PEEK nanofiltration membranes with very low sulfonation approaching the level of native PEEK. The degree of sulfonation was calculated as follows:

$$Degree\ of\ Sulfonation = \frac{S_E}{S_T} * 100 \qquad (1.1)$$

where S_E is the measured weight-percent sulfur to carbon ratio and S_T is the theoretical weight-percent sulfur to carbon ratio for 100 percent sulfonated PEEK. They reported all native PEEK blends from suppliers had less than 3 percent sulfonation, but the final

membranes produced all had at least double the degree of sulfonation of the original native material. Their work also indicated that increasing the degree of sulfonation decreased the chemical resistance of S-PEEK to several solvents.

All these solvent-based techniques have abundant potential for future inquiry, but they all focus on forming membranes from porous films rather than by forming discrete fibers.

Research has been made into electrospinning S-PEEK to form discrete fibers. For example, S-PEEK fibers down to a diameter of about 100 nanometers have been manufactured and characterized by Sadrjahani, *et al.* [11], where such fibers have a degree of sulfonation of over 60 percent. However, at the time of this thesis no published research has been found regarding the potential for electrospinning native PEEK fibers without increasing the degree of sulfonation.

1.3 – Electrospinning

Electrospinning is the process of using an applied electric field to draw a polymer into a fiber. The diameter of electrospun polymer fibers can range from millimeters down to the order of tenths of nanometers [12]. In order for the polymer to flow freely into a fiber, it must be in a fluid state. This is commonly achieved by two different methods: solution electrospinning and melt electrospinning.

In solution electrospinning methods, the given polymer is mixed into a solvent so that it forms a viscous fluid during the spinning process. The solution is then forced from a syringe through a needle tip, or spinneret, forming a droplet at the end of the spinneret [12,13]. A high voltage is then applied to the spinneret and a grounded conductive collector is placed a short distance away. The distance from the spinneret to the collector is known as the "working distance". The surface tension force holds the droplet at the end of the

spinneret in a roughly spherical shape. However, when a high voltage is applied to the spinneret, charges accumulate on the spinneret tip and the droplet. These charges repel each other, causing the droplet to extend out away from the spinneret. At a critical charge density, associated with the applied voltage, the polymer forms a distinct Taylor cone shape and is then drawn to the grounded collector where it solidifies as the solvent evaporates [12].

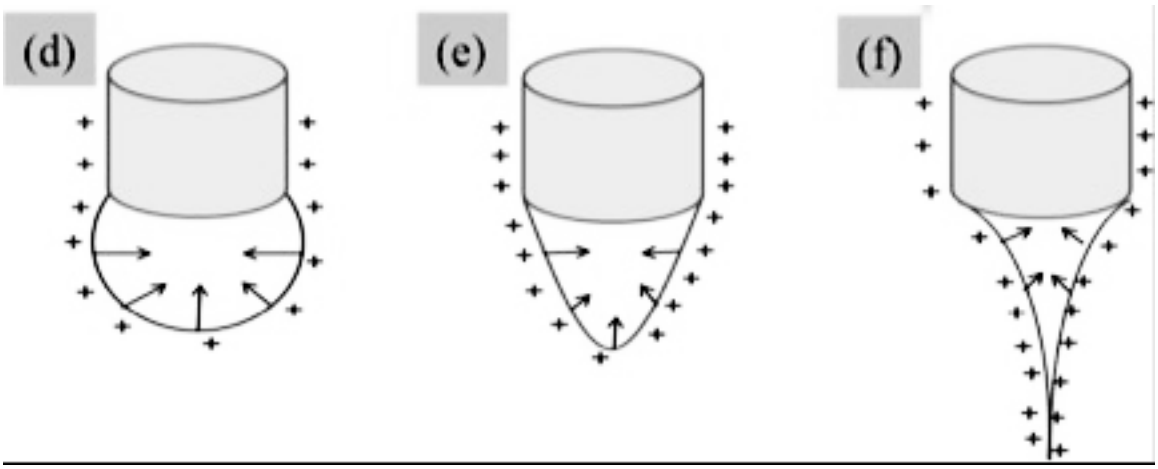

Figure 1.3: A polymer droplet on the end of a spinneret (shown as a gray cylinder): (d) spherical shape under surface tension alone, (e) accumulation of charges and the beginning of shape deformation, (f) a critical charge density resulting in Taylor cone formation (image from [9]). In this example, the high-voltage is applied to the spinneret.

In melt electrospinning methods, the polymer is raised to a temperature above its melt transition. At this point, the polymer can be extruded from a needle in the same manner as in solution electrospinning or can be drawn from a reservoir of molten polymer in other creative ways depending on the application. For example, a rotating wheel in a reservoir of molten polymer as well as a simple droplet of molten polymer suspended on a needle tip have been shown to be simple but effective ways of producing fibers [14,15,16]. The significant challenge in melt electrospinning as compared to solution electrospinning is

the need to keep the polymer molten throughout the spinning process. In research done by Kong, *et al.* [17] the polymer is heated in a reservoir and then extruded from the spinneret while the air between the spinneret and collector is also kept at a high temperature. The longer the polymer is in a fluid melt state, the longer it can be subjected to the force of the electric field. This force can induce a whipping and stretching action that has been shown in multiple studies to decrease fiber diameter [17, 18]. However, a significant challenge exists in melt electrospinning to prevent the applied high voltage from interfering with the system used to heat the polymer. Commonly used resistive heating systems rely on a high current being passed through a conductor to produce heat, and applying a high voltage to this system could interfere with or damage the heater. One effective solution is to apply the high voltage to the collector and to ground the polymer spinneret. In this way, the electrostatic charges are reversed in polarity but still capable of attracting the polymer to the collector [14,16,18]. Positive charges accumulate on the collector and induce an accumulation of negative charges at the end of the spinneret through electrostatic induction [19].

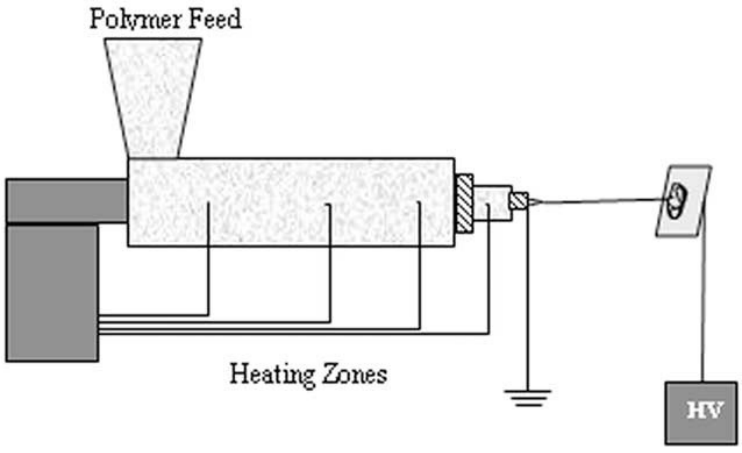

Figure 1.4: A typical melt electrospinning setup where the polymer is heated to a liquid state, extruded from a grounded needle, and drawn to the right towards a collector plate with an applied high voltage (image from [16]).

1.4 – Electrospun Fibers and Applications

On its own, the usefulness of a single electrospun fiber is fairly limited. However, when several fibers are deposited on top of one another, they form a porous membrane or fiber mat. The fibers in such a mat can be randomly oriented on top of one another, or have two and even three-dimensional alignment depending on the method of collecting the fibers [8]. For example, a fixed collector will collect randomly oriented fibers, a result of the instability of the polymer jet as it travels through the air to the collector [20]. A rotating collector wheel however, will generally orient the fibers in the direction of rotation within a certain margin of error, as the polymer jet will always show some instability. In more sophisticated setups, direct writing of polymers, a process much like 3-D printing, is possible by having the spinneret very close to a flat collector moving in an x-y plane (see Figure 1.5).

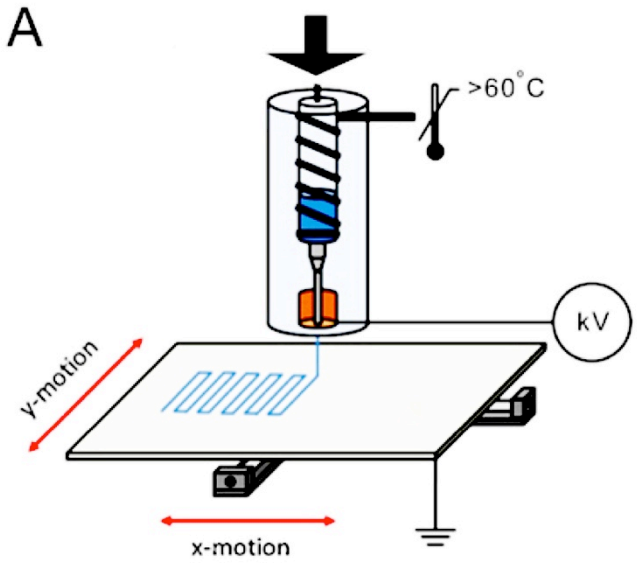

Figure 1.5: A direct writing melt electrospinning setup (image from [3]).

By direct writing, fiber mats can be organized in two and three dimensions. Therefore there is the potential for electrospun fibers to be utilized in diverse applications, but the scope of this thesis will be limited to fibers oriented randomly on a flat collector.

As was stated previously, randomly oriented fibers form a fiber mat that behaves like a porous membrane. Because of this, one of the most direct applications of electrospun fibers is for use as a filtration membrane for both gases and liquids. These ultrafine fibers have unique and desirable properties due to their small diameter. First, they have a high surface-area to volume ratio, meaning that any material passing through the fiber mat must interact with a greater amount of surface area than a similar volume of larger structures. This is useful for filtration applications where a reagent, such as metal nanoparticles, can be applied to the surface of the fibers to selectively bind and trap toxins [8]. Second, electrospun fibers form fiber mats with an adjustable porosity down to the Nano scale. This is widely applicable in different industrial applications in instances where gases and liquids must have large particles removed and smaller particles passed through. For example, electrospun fiber mats can be used to pre-filter water going in to a reverse osmosis sytem. The polymer mat traps the larger contaminants that would otherwise pass into the delicate filtration system, lowering maintanace costs and increasing the overall efficiency of the system [3].

Electrospun PEEK is therefore an exceptional candidate for filtration applications. Its resistance to almost all common solvents means it could be applied to solvent filtration, and existing research performed using non-electrospun PEEK filters supports this as a viable use [9]. Furthermore, PEEK's mechanical and thermal durability means that it can outperform membranes formed from other polymeric materials in high temperature and high stress environments, such as high temperature exhaust gas filtration or high flow rate fluid filtration [9].

1.5 – Electrospinning PEEK

The unique challenges associated with electrospinning PEEK are a direct result of its exceptional chemical, thermal, and mechanical properties. As was stated in Section 1.2, PEEK has not been dissolved in Sulfuric Acid without increasing its degree of sulfonation. Consequently, solution electrospinning to achieve native unsolfonated PEEK is not currently possible. Therefore, the first challenge is to prepare unsulfonated PEEK that can be electrospun. A clear solution to this problem is to use the melt electrospinning technique as it eliminates the need for a solvent. However, this on its own presents a second challenge due to PEEK's very high melting point of 343 °C. The melt electrospinning apparatus must be able to raise the source quantity of PEEK above this temperature and also keep its temperature elevated while the fibers travel to the collector. Ideally, the PEEK should gradually cool on its way to the collector so that it develops a fibrous shape and is no longer fully molten when it lands on the collector. Otherwise any PEEK that hits the collector in a molten state is prone to forming droplets rather than fibers, as has been observed in similar polymers [17].

The third main challenge associated with melt electrospinning PEEK is its very high melt viscosity compared to other polymers. PEEK has a melt viscosity that ranges from 90 to 475 Pa.s, where a higher viscosity correlates to a higher molecular weight, meaning that even in its molten state PEEK has a high resistance to flow. Similar research has shown that polymers of this viscosity range can be electrospun, but require an apparatus capable of significantly higher electric field strength compared to solution electrospinning to overcome the intermolecular forces and draw the polymer into a fiber [3,14,18]. For example, Lyons, *et al.* [16] compared electrospinning different molecular weight forms of Polypropylene. They found that at sufficiently high molecular weights –and thus melt viscosities- a Taylor cone was not formed at the spinneret even at the highest possible

electric field strengths. Rather, the polymer was slowly extruded from the spinneret without changing its diameter. Furthermore, at very low molecular weights it was possible for the polymer jet to become too instable and break up before hitting the collector. Therefore, it is necessary to choose an appropriate grade of PEEK with correct molecular weight and viscosity to successfully form fibers. The choice of PEEK grade will be discussed in full detail in Chapter 2.

Additionally, a balance must be struck between applied voltage and distance from the collector. The factor limiting the electric field strength, commonly measured in kV/cm, is the breakdown voltage of air. When the limit of breakdown is reached, the ambient air in the region between the spinneret and collector (this region is also referred to as the "spin line") can no longer act as an insulator and the high voltage is able to pass from the collector to the grounded spinneret or vice versa, causing an undesirable electrical arc. At normal atmospheric conditions this is roughly 30 kV/cm over small gaps. However, air pressure and temperature both affect this value. Breakdown voltage, U, varies with temperature, T, and pressure, p, in the following way [21]:

$$U \propto \frac{p}{T} \tag{1.2}$$

From Equation 1.2, it is clear that an increase in temperature will result in a decrease in breakdown voltage at constant pressure. Given that the melt electrospinning apparatus will be operating at very high temperatures, an appropriate balance between working distance and applied voltage must be established to provide sufficient force on the polymer without causing electrical breakdown of the air.

1.6 – Validating Results

The primary methods for analyzing the quality of electrospun fibers are polarized optical microscopy (POM) and scanning electron microscopy (SEM). These methods allow

for a direct visualization of the diameter, quality, alignment, and quantity of fibers produced. Other secondary methods can be used to determine thermal and organizational properties of the molecules in the fibers and make it possible to guarantee that the collected fibers are made of PEEK and not the result of other unwanted sources. Secondary methods used to characterize other electrospun polymers include: Differential Scanning Calorimetry (DSC) and Thermogravimetric Analysis (TGA) to observe the thermal properties, as well as Fourier Transform Infrared Spectroscopy (FTIR) and X-Ray Diffraction (XRD) to observe molecular and crystalline structure [11].

Chapter 1 References:

[1] Fink JK. Chapter 6 - Poly(aryl ether ketone)s, High Performance Polymers (Second Edition) (2014), In Plastics Design Library, William Andrew Publishing, Pages 153-175. ISBN 9780323312226. Doi: 10.1016/B978-0-323-31222-6.00006-6.

[2] Victrex plc. Victrex 150G Datasheet, Victrex Plc, July 2017.

[3] Brown T, Dalton P, Hutmacher D. Melt electrospinning today: An opportune time for an emerging polymer process, Progress in Polymer Science (May 2016), Volume 56, Pages 116-166. ISSN 0079-6700. Doi: 10.1016/j.progpolymsci.2016.01.001.

[4] Panayotov I, Orti V, Cuisinier F, Yachouh J. Poly(ether ether ketone) (PEEK) for medical applications, Journal of Materials Science: Materials in Medicine (2016), Volume 27 Issue 118, Pages 1-11. Doi: 10.1007/s10856-016-5731-4.

[5] Patel P, Hull R, McCabe R, Flath D, Grasmeder J, Percy M. Mechanism of thermal decomposition of poly(ether ether ketone) (PEEK) from a review of decomposition studies, Polymer Degradation and Stability (2010), Volume 95, Issue 5, Pages 709-718. ISSN 0141-3910. Doi.: 10.1016/j.polymdegradstab.2010.01.024.

[6] Gil M, Ji X, Li X, Na H, Hampsey E, Lu Y. Direct synthesis of sulfonated aromatic poly(ether ether ketone) proton exchange membranes for fuel cell applications, Journal of Membrane Science (2004), Volume 234, Issues 1–2, Pages 75-81, ISSN 0376-7388. Doi: 10.1016/j.memsci.2003.12.021.

[7] Koziara BT, Kappert EJ, Ogieglo W, Nijmeijer K, Hempenius MA, Benes N. Thermal stability of sulfonated Poly(ether ether ketone) films: on the role of protodesulfonation, Macromolecular Materials and Engineering (2016), Volume 301, Pages 71–80. Doi: 10.1002/mame.201500075.

[8] Ramakrishna S, Fujihara K, Teo WE, Yong T, Ma Z, Ramaseshan R. Electrospun nanofibers: solving global issues, Materials Today (2006), Volume 9, Issue 3, Pages 40-50. ISSN 1369-7021. Doi: 10.1016/S1369-7021(06)71389-X.

[9] da Silva Burgal J, Peeva L, Kumbharkar S, Livingston A. Organic solvent resistant poly(ether-ether-ketone) nanofiltration membranes, Journal of Membrane Science (2015), Volume 479, Pages 105-116. ISSN 0376-7388. Doi: 10.1016/j.memsci.2014.12.035.

[10] Mehta R. Development of microporous membranes from Poly(ether ether ketone) [PEEK] via thermally-induced phase separation [TIPS], Ph. D. Thesis, 1996, University of Kentucky.

[11] Sadrjahani M, Gharehaghaji AA, Javanbakht M. Aligned electrospun sulfonated polyetheretherketone nanofiber based proton exchange membranes for fuel cell applications, Polymer Engineering Science (2015), Volume 57, Pages 789–796. Doi: 10.1002/pen.24453.

[12] Haider A, Haider S, Kang IK. A comprehensive review summarizing the effect of electrospinning parameters and potential applications of nanofibers in biomedical and biotechnology, Arabian Journal of Chemistry (2015), Volume 8, Issue 16, Pages 1-24. ISSN 1878-5352. Doi: 10.1016/j.arabjc.2015.11.015.

[13] Dalton P, Vaquette C, Farrugia B, Dargaville T, Brown T, Hutmacher D. Electrospinning and additive manufacturing: converging technologies, Biomaterial Science (2013), Volume 1, Issue 2, Pages 171-185, The Royal Society of Chemistry. Doi: 10.1039/C2BM00039C.

[14] Niu H, Lin T, Wang X. Needleless electrospinning. I. A comparison of cylinder and disk nozzles, Journal of Applied Polymer Science (2009), Volume 114, Issue 6, Pages 3524-3530. Doi: 114. 3524-3530. 10.1002/app.30891.

[15] Fang J, Zhang L, Sutton D, Wang X, Lin T. Needleless melt-electrospinning of polypropylene nanofibres, Journal of Nanomaterials (2012), Volume 2012, Pages 1-9. Doi: 10.1155/2012/382639.

[16] Lyons J, Li C, Ko F. Melt-electrospinning part I: processing parameters and geometric properties, Polymer (2004), Volume 45, Issue 22, Pages 7597-7603. ISSN 0032-3861. Doi: 10.1016/j.polymer.2004.08.071.

[17] Kong CS, Jo KJ, Jo NK, Kim HS. Effects of the spin line temperature profile and melt index of poly(propylene) on melt-electrospinning, Polymer Engineering Science (2009), Volume 49, Pages 391–396. Doi: 10.1002/pen.21303.

[18] Cho D, Zhmayev E, Joo YL. Structural studies of electrospun nylon 6 fibers from solution and melt, Polymer (2011), Volume 52, Issue 20, Pages 4600-4609. ISSN 0032-3861. Doi: 10.1016/j.polymer.2011.07.038.

[19] Saslow W. Chapter - 1, A history of electricity and magnetism, to conservation of charge, 'Electricity, Magnetism, and Light', Academic Press (2002), San Diego, Pages 39-79, Doi: 10.1016/B978-012619455-5.50001-2.

[20] Li Z, Wang C. Chapter – 2, Effects of working parameters on electrospinning, 'One-Dimensional Nanostructures', Springer Briefs in Materials (2013), Pages 15-28. Doi: 10.1007/978-3-642-36427-3_2.

[21] Allen NL. Chapter – 20, Fundamental aspects of air breakdown, 'High Voltage Engineering and Testing', Energy Engineering (2001), 2nd ed., IET Digital Library, Pages 581-600. Doi: 10.1049/PBPO032E_ch20.

Chapter 2 – Experiment

2.1 – Polymer Choice

Research into the different molecular weight grades of PEEK revealed a range of available viscosities from 90 Pa.s to 475 Pa.s, as shown in Table 2.1. A comparison showed that generally they shared the same properties with the exception of tensile elongation at break, impact strength, and -of course- viscosity. However, the most important properties for filtration applications such as solvent resistance, tensile strength, and thermal resistance are largely unchanged for different molecular weights [1,2,3].

Table 2.1: A comparison of properties of different molecular weight grades of PEEK [1,2,3].

Property	Victrex 150G	Victrex 450G	Victrex 650G	Units
Tensile Strength	105	98	95	MPa
Tensile Elongation	30	45	60	% At Break
Tensile Modulus	4.1	4.0	3.9	GPa
Charpy Impact Strength	4.2	7.0	10	kJm^{-2} Notched
Melt Viscosity	130	350	475	Pa.s
Melt Temperature	343	343	343	Degrees C

Reviews of polymers that have been successfully melt electrospun gave a reasonable range of target melt viscosities, shown in Table 2.2.

Table 2.2: A comparison of properties of high-viscosity melt-electrospun polymers similar to PEEK [4,5,6,7].

Polymer	Melt Viscosity (Pa.s)	Melt Temperature (°C)	Electric Field (kV/cm)
PP[a]	75	270	5
Nylon-6	192.5	224	2-2.8
PCL[b]	291.5	60	1-4
PLA[c]	120	165	.5-3

a. Polypropylene; b. Polycaprolactone; c. Polylactic acid

It was determined that to have the best chance of success within the time frame of this thesis, the lowest molecular weight PEEK, Victrex 150G, should be chosen as it lies safely within the range of viscosities from successful related experiments, at 130 Pa.s.

2.2 – Temperature

A few methods were attempted to achieve the high temperatures necessary to melt and electrospin PEEK. One method used an electrically insulated resistive heating wire to heat a cylindrical polymer reservoir and extrude the polymer out of the end of the cylinder like a spinneret (see Figure 2.1). However, this method was deemed undesirable due to the observation that even though the inside of the cylinder could achieve the necessary temperature, any polymer exiting the cylinder would cool and solidify much too quickly in the absence of any additional source to heat the spin line air. This determination was made by using a type K thermocouple to measure the temperature of the cylinder and the region of spin line air just in front of the cylinder opening.

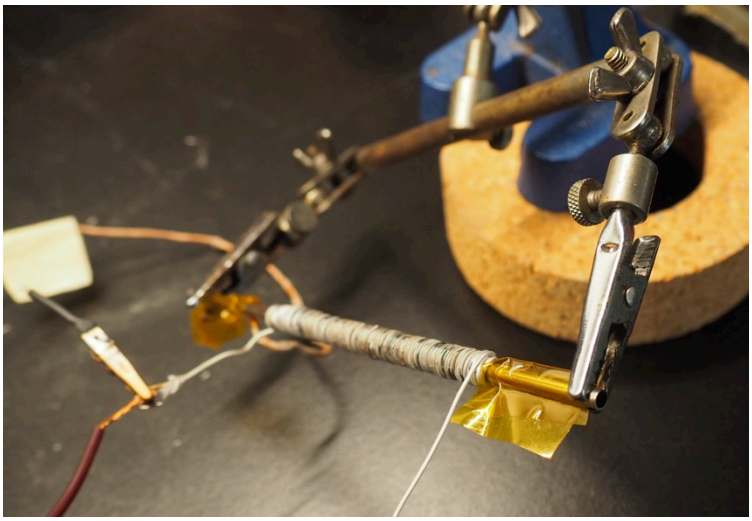

Figure 2.1: A cylindrical spinneret design with resistive heating wire wrapped around its surface.

A second method addressed the issue of heating the spin line air by putting the melt portion of the apparatus inside a Thermolyne 2000 model furnace, capable of reaching a temperature of 1200 °C (see Figure 2.2). It was determined that since the furnace was capable of raising the polymer and the spin line air to sufficient temperature, this method was chosen to heat the polymer throughout the rest of this thesis.

In order for the PEEK polymer to be melted and then cooled on the collector, the collector had to be at a significantly lower temperature than the spinneret and spin line. Therefore, the collector could not feasibly be located inside the furnace but had to be positioned outside to allow for a temperature gradient. To allow the fibers to travel from the spinneret to collector outside the furnace, the original furnace door was replaced with a custom door milled from ¼ inch MACOR ceramic (Corning Incorporated, Corning NY). This door was both thermally and electrically insulating and capable of withstanding the high temperatures required by this experiment. It door featured a ¼ inch diameter hole in the bottom left corner for the spinneret wire to enter the furnace and a 2.5 inch diameter hole in its center through which the fibers could exit the furnace and travel to the collector.

Figure 2.2: Confirming the furnace temperature dial calibration with the type K thermocouple. The original furnace door is still in place.

2.3 – Electric Field

A DC high-voltage power supply (Gamma High Voltage Research, Model ES30P, Ormond Beach, FL) capable of delivering 30 kV was used to provide the driving electrostatic force necessary for electrospinning. Research of successful melt-electrospinning with polymers of similar viscosity suggested an electric field strength range of 1-5 kV/cm (see Table 2.2) [4,5,6].

Initially, the more standard approach of applying the high-voltage to the spinneret and grounding the collector was tested at room temperature using a stainless steel 20 gauge wire in place of the spinneret. The rest of the copper wiring inside the furnace was insulated with ceramic beads (see Figure 2.3). However despite the fact that the Thermolyne furnace was lined with firebrick over most of its interior, upon reaching approximately 5kV the high voltage spinneret began to short to components within the furnace. It was concluded that the heating elements were not adequately shielded from the high voltage and were the most

likely location of the short from high voltage to ground. In order to avoid this issue, the voltage was instead applied to the collector, which could be placed an adequate distance away from the oven to avoid electrical shorting issues. With the same setup as before and the high voltage applied to the collector, the maximum voltage of 30 kV was safely applied at a distance of 6 cm without any electrical discharge. Therefore for the rest of the thesis the high voltage was applied to the collector outside the furnace rather than the spinneret.

Figure 2.3: The wiring layout inside the furnace for both cases where the spinneret was either at high voltage or grounded. The 20 Ga. stainless steel spinneret wire was held in a solid-copper supporting bracket. A 20 Ga. solid copper wire connected the copper bracket to a 14 Ga. solid copper wire insulated with ceramic beads. The rest of the wiring out of the furnace to ground consisted of 14 Ga. solid copper wires.

2.4 – Spinneret

The most common choice of spinneret in melt electrospinning applications is a hollow needle through which the molten polymer is extruded. This technique requires an applied force, typically supplied by a screw or plunger extruder, to force the polymer to the tip of the spinneret. Due to the fact that the entire spinneret assembly had to be located

within the furnace, all components had to be able to withstand temperatures in excess of 343 °C. This therefore ruled out using any conventional mechanical extruder, as it would not be able to withstand the extreme temperatures inside the furnace. Without an extruding force acting on the polymer, the choice of a needle as spinneret was deemed untenable.

Still, at its most basic level, a spinneret must simply be a location where the molten polymer can form a Taylor cone during spinning. For example, Lyons, *et al.* [8] reported a successful technique using the simplest spinneret. They placed a portion of Polypropylene directly onto a 1.5 mm needle tip to melt without any extruding force acting on the polymer. The surface tension of the molten Polypropylene droplet kept it in a roughly spherical shape on the end of the needle. The molten droplet then formed a Taylor cone under the applied voltage, but as the cone decreased in volume the fibers decreased in diameter. No polymer was extruded to replenish the Taylor cone. This is a clear downside to this choice of spinneret; the Taylor cone decreases in size as more and more polymer is drawn from the source, which could lead to inconsistent fiber diameter over a long duration of electrospinning. However, it was proposed for this thesis that as long as a sizable portion of source polymer was placed at the end of the spinneret then the volume of polymer drawn to the collector would have an insignificant effect of the shape of the Taylor cone provided the duration of the electrospin was kept sufficiently short. With this assumption in place, two spinneret designs were investigated. One was a 20-gauge stainless steel wire (see Figure 2.3) and the second was a tungsten wire basket (Ted Pella Inc. Cat# 72-2) (see Figure 2.4).

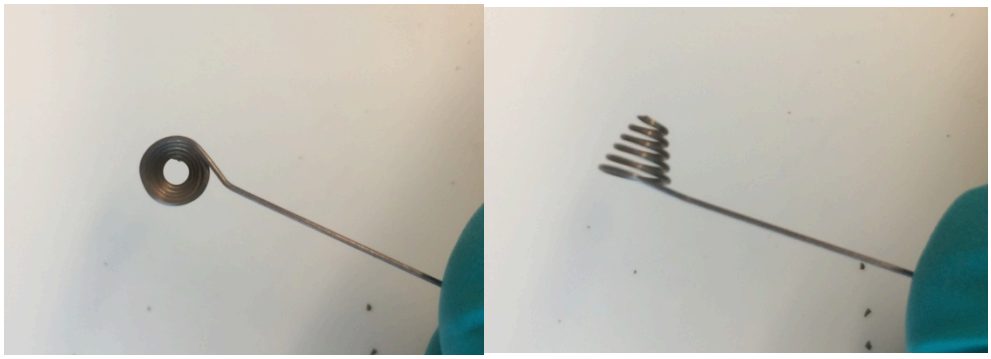

Figure 2.4: The Tungsten wire basket with hole trimmed at the bottom.

Preliminary testing showed that the tungsten basket was unable to form a Taylor cone. Although the polymer flowed down to the opening at the bottom of the basket it showed no evidence of being drawn out by the applied high voltage even at its highest level. This is likely a result of the high surface area of the basket combined with the high viscosity of the polymer. The polymer tended to flow into the grooves between the basket wires and cling there rather than flowing out through the bottom hole. Even after using a wire to manually force a polymer droplet out through the bottom hole, the polymer tended to be drawn back up into the basket. All this evidence indicated that the electrostatic force required to overcome the surface tension was greater than what this apparatus is capable of producing (see Figure 2.5).

Figure 2.5: The Tungsten basket as viewed through the furnace door after an attempted spin. No Taylor cone is produced from the opening at the bottom of the basket.

The stainless steel wire however, was capable of suspending a droplet of molten PEEK and forming a Taylor cone under the influence of an applied high voltage. This was abundantly clear by observing the shape of the cooled PEEK droplets after spinning (see Figure 2.6). Therefore, this spinneret design was chosen for the final experimental setup of this thesis.

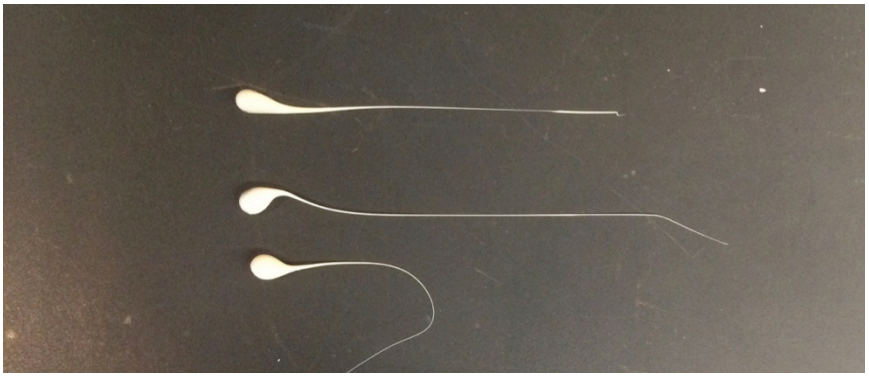

Figure 2.6: Three PEEK droplets after cooling and being removed from the spinneret. They each show the Taylor cone shape and a long PEEK fiber being drawn off.

2.5 – Collector

As stated in Section 1.3, several options exist for the conductive collector. However, a simple and well-researched option is Aluminum foil. With applied voltages of up to 30 kV being applied to this collector, considerations had to be made to minimize occurrences of electrical discharge. First, the foil collector was applied to the face of a 50 mm by 75 mm dimension glass slide of 1 mm thickness using 3M DuPont "Kapton" polyimide film tape. This 1 mil, or 0.001 inch thick, Kapton film tape has a dielectric strength of 7000 Volts per mil and is capable of withstanding temperatures of at least 260 °C [9]. Using this tape enabled the foil to be pulled taut along the face of the glass, preventing charge accumulation along any wrinkles in the foil surface. Second, it was found that having exposed sharp edges of the foil caused audible and visible blue electrical discharge in the surrounding air. This "corona discharge" was a result of avalanches of ionizing electron collisions in the air around the sharp edges of the collector [10]. Corona discharge is generally undesirable in electrospinning as it represents a location susceptible to unsafe electrical breakdown, or arcing, and can damage components such as the Kapton tape supporting the collector [11]. To prevent corona discharge, the Aluminum foil was cut to have only curved edges, and all edges of the foil were covered with two to four layers of insulating Kapton Tape depending on the applied voltage (see Figure 2.7). This technique proved sufficient to prevent corona discharge at voltages of up to 30 kV.

Third, the collector plate was electrically insulated from its surroundings by being taped to a specially designed insulating stand. This stand consisted of a wooden arm covered in a wrapping of Teflon film and Kapton tape. This wooden arm was then attached to a metal pole with an acrylic base that was placed on a one-inch Teflon sheet. By taping the collector and glass backing plate to the Teflon and Kapton wrapping, the collector was

sufficiently insulated to prevent any chance of grounding to its surroundings at high voltages (see Figure 2.8).

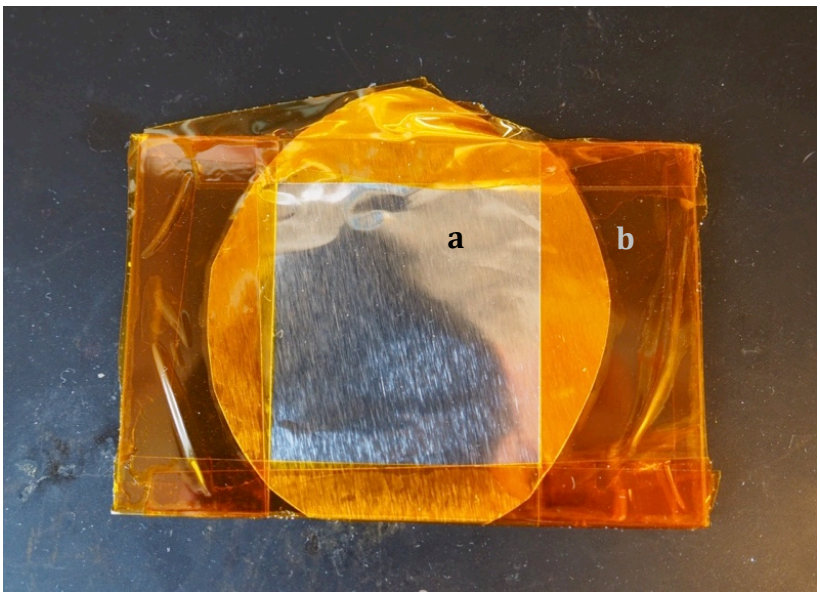

Figure 2.7: The Aluminum foil collector (a), shown with its curved edges and Kapton insulating tape (b) on a glass slide backing (underneath and not visible).

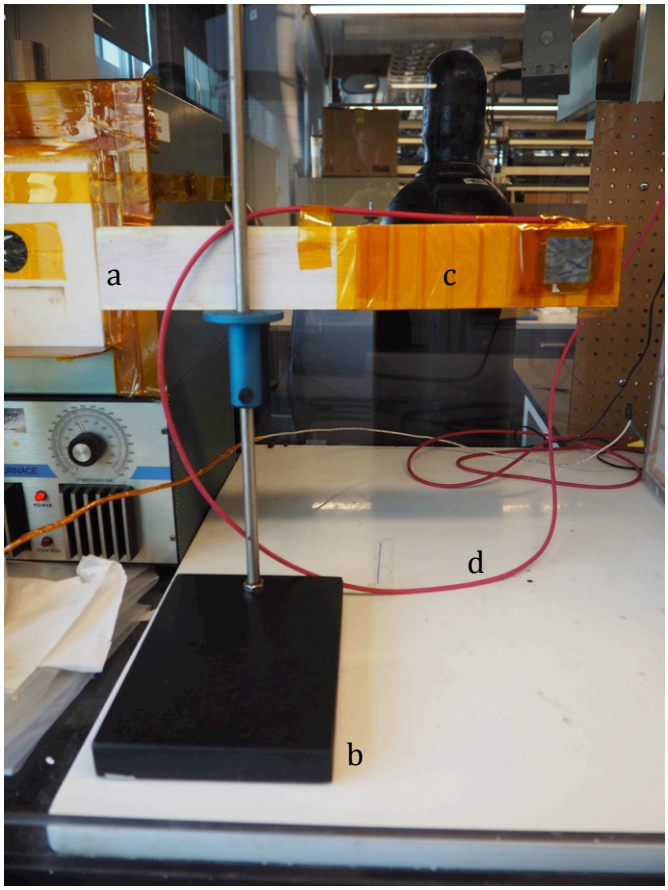

Figure 2.8: The collector mounted on the electrically insulating stand, shown with its wooden supporting arm (a), acrylic and Teflon bases (b), and insulating wrap (c). The red wire (d) supplies the high-voltage and is shielded by insulation rated to 40 kV.

2.6 – Working Distance

As introduced in Section 1.1, the working distance refers to the distance between the spinneret and the collector. At a constant applied voltage, an increase in working distance correlates to a decrease in electric field strength in accordance with Coulomb's Law [12]. It states that the electrostatic force, F, between charged particles separated by a distance, r, follows:

$$F \propto 1/r^2 \tag{2.1}$$

With target electric field strengths of 1-5 kV/cm, there were a number of possible combinations of applied voltage and working distance that would produce this field strength. Yet, some other factors had to be considered in making this decision.

First, the limit for the DC power supply was 30 kV. In order to achieve 5 kV/cm the working distance could not exceed 6 cm. It would have been possible to use a power supply capable of higher applied voltages, but this would have introduced additional concerns. The collector could not have been placed too far away from the opening of the furnace as the fibers would cool prematurely and not stick to the collector as intended. Additionally, at higher voltages, the collector would be more prone to corona discharge as well as arcing to the furnace and other surroundings. Therefore, to ensure an effective and safe procedure, the voltage was chosen not to exceed 30 kV.

Second, a longer working distance generally correlates to a decrease in fiber diameter. The research of Kong, *et al.* [13] as well as Fang, *et al.* [14} suggests that this is possibly a result of a non-uniform electric field along the spin line. Variance in the electric field acting on the charged polymer fiber as it moves to the collector could cause the fiber to be elongated at different rates and stretched. More time and distance subjected to this stretching therefore correlates to a finer fiber diameter. However, the model of electrospinning with the voltage applied to the collector is not fully explicated in literature and will require further inquiry beyond the scope of this thesis.

With a desire to minimize fiber diameter, achieve an appropriate cooling rate of the fiber through the air, and maintain the desired electric field strength, the working distance was chosen to be in the range of 3 to 5 cm. This is in good accordance with the work of Lyons, *et al.* [8], whose spinneret design most closely resembled the spinneret used in this thesis and whose working distance was in the range of 2 to 5 cm. It is therefore expected

that the smallest fibers should occur at the longest working distance, 5 cm, so long as they do not cool too rapidly.

A detail of working distance pertinent to the design of this thesis is that the working distance must be split into two parts: the distance from the spinneret to the furnace door opening and the distance from furnace door opening to the collector. It was observed with a thermocouple that there was a steep temperature gradient near the opening in the furnace door. Consequently, the polymer cooled and solidified almost instantly when exposed to the air temperature outside the furnace. In order to find a suitable distance from furnace door to collector, preliminary PEEK electrospinning was conducted, first with the collector directly against the furnace door. However, at this distance, the air temperature was high enough to degrade the silicone adhesive on the Kapton tape and the collector began to come apart. Therefore, the collector was moved back to roughly 1 cm from the furnace door for subsequent tests. At this distance, the fibers cooled sufficiently to form their fibrous shape and did not show any signs of continued melting while on the collector. This meant that they retained their fibrous shape indefinitely while on the collector. With this evidence, the distance from furnace door to collector was kept at 1 cm for the remainder of the thesis, with an error of ±0.1 cm due to the foil collector not being perfectly flat or perpendicular to the spinneret. The varied aspect of the working distance was the distance from the spinneret to the furnace door.

2.7 – Full Experimental Setup

The following section lays out the steps necessary to perform the experimental procedure of melt electrospinning PEEK.

1) The spinneret assembly was placed inside the furnace (see Figure 2.10). The ground wire was connected to the main electrical grounding line with an alligator clip. The continuity from ground to the spinneret tip was checked with a multimeter.

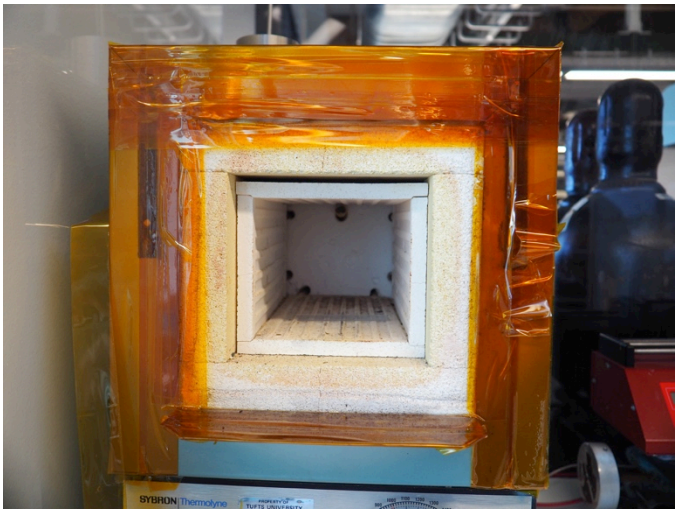

Figure 2.9: The empty furnace before the spinneret is placed inside. The exterior of the furnace is insulated with several layers of Kapton tape.

2) The spinneret was adjusted to the appropriate working distance from the outside of the furnace door and centered in the furnace door opening. The working distance was measured with a measuring tape precise to 1 mm (see Figure 2.11).

Figure 2.10: The spinneret distance being measured with the measuring tape. Note the furnace door is a custom milled piece of 1/4" MACOR ceramic held in placed by a Kapton strip under tension.

3) The furnace was turned on and set to the appropriate temperature between 500 and 600 °C depending on the working distance. The furnace was allowed time to reach its set point and the temperature at the spinneret tip was measured with a thermocouple (see Figure 2.12). If the temperature was not between 350 and 375 °C then the set point was adjusted as necessary and the furnace was given time to re-equilibrate. It was observed that prolonged exposure of the PEEK droplet to temperatures in excess of 390 °C did not result in fibers. To be precise, holding the PEEK droplet above this temperature for more than 30 minutes caused the exterior of the droplet to become tacky and resist flow due to some form of surface degradation. To avoid this, the temperature at the spinneret was closely monitored and kept below this threshold.

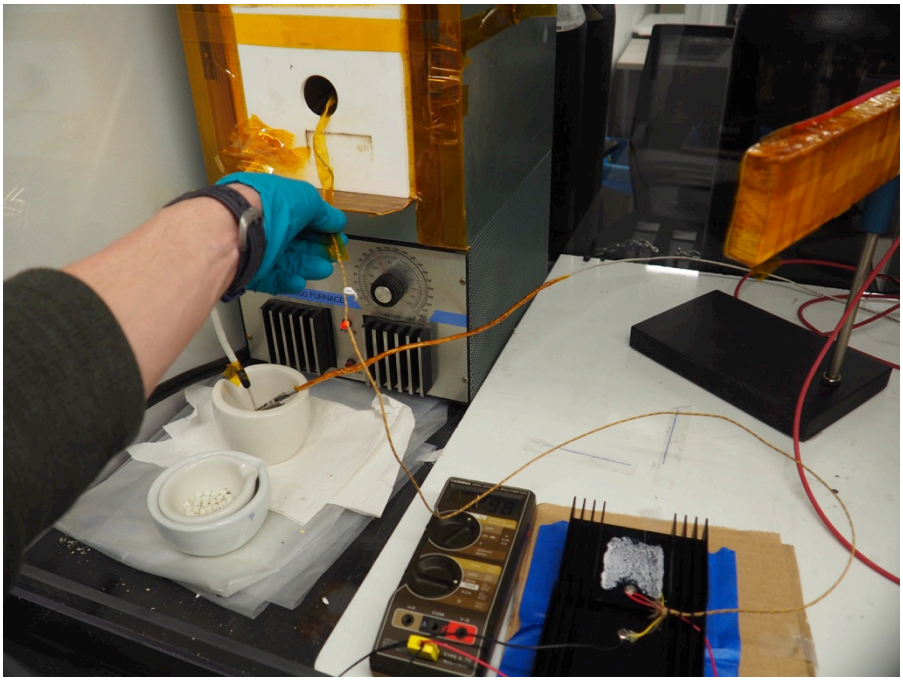

Figure 2.11: The spinneret temperature being measured with the type K thermocouple.

4) Once at temperature, a pellet of PEEK was placed into contact with the spinneret using tweezers. The pellet tended to stick to the spinneret after a few seconds. The pellet was then gently nudged on top of the spinneret where it melted into a droplet.

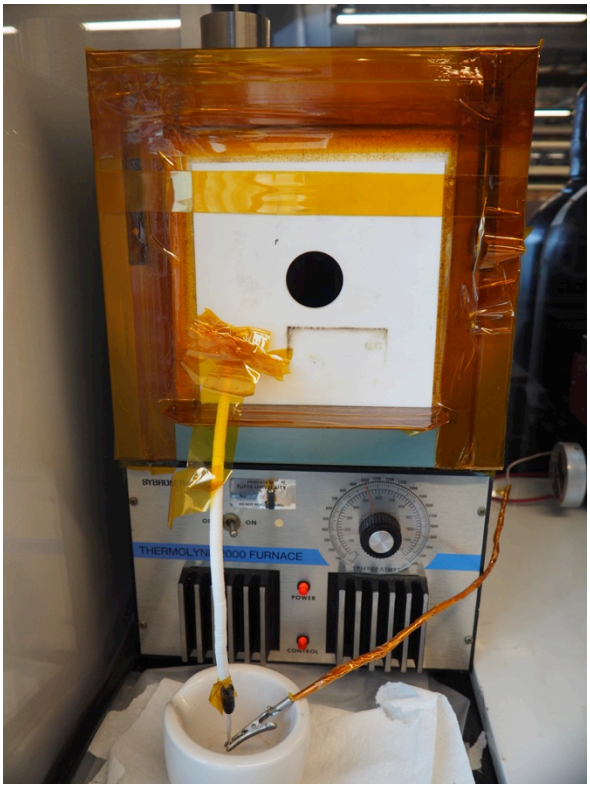

Figure 2.12: The layout of the furnace and MACOR ceramic door prior to the collector being put in place. Note the grounded wire insulated by ceramic beads and Kapton tape.

5) With the droplet in place on the spinneret, a collector was fastened to the supporting arm and the high voltage line was attached to the collector, all using Kapton tape. The continuity from the collector to the end of the high voltage line was then checked with a multimeter.
6) The collector was brought 1 cm away from the furnace door and centered on the opening. This distance was also measured with a tape measure precise to 1 mm.
7) With the spinneret, PEEK, and collector all in place, the high voltage line was connected to the DC power supply and the doors to the fume hood were closed for safety. The exhaust function of the fume hood was switched off for the experiment to reduce the effects of turbulent air.

8) The DC power supply was then switched on and ramped up from zero to the appropriate voltage over the span of a few seconds using the control knob. If any arcing to the spinneret or surroundings was observed then the power supply was immediately shut off and the experiment repeated from step 4 after inspecting for any damaged components.

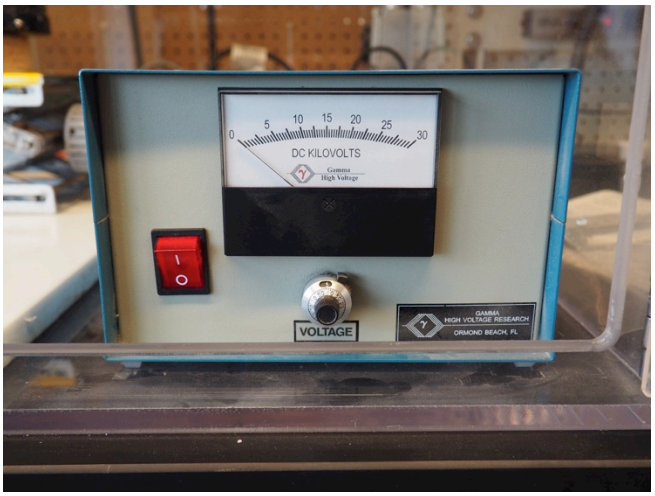

Figure 2.13: The DC power supply before being turned on. Note the voltage control knob located in the center.

9) In the case where there was no arcing, the spin was allowed to proceed at the set voltage for a period of 5-10 minutes. This spin duration allowed for ample production of fibers without a significant volume loss from the spinneret droplet.

10) After the spin was completed, the power supply was shut off and the collector was inspected with a flashlight for evidence of fibers. It was critical to inspect for fibers before moving the collector as sometimes the fibers which had been stopped mid flight between the spinneret and collector would still be connected to both the spinneret droplet and the collector. Moving the collector could cause the fibers to be pulled off the

collector and lost. Therefore, prior to moving the collector, any interstitial fibers were cut with sharp scissors.

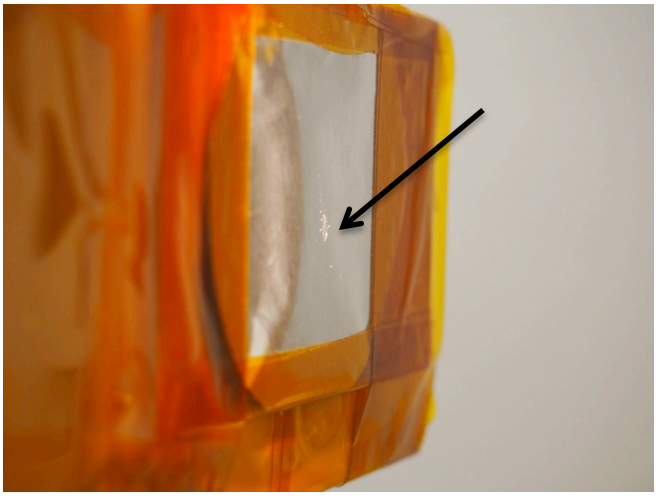

Figure 2.14: Inspecting the collector after a spin. Note the fibers in the center of the foil but no interstitial fibers still connected to the spinneret.

11) Finally, the collector was removed from the supporting arm and saved for later analysis.
12) For subsequent spins while the furnace was at temperature, the spinneret was trimmed with wire cutters through the furnace door opening, the spinneret working distance was reset to the appropriate distance, and a new pellet of PEEK was applied to the spinneret tip. With a new collector, steps 5-11 were then repeated for each spin.
13) After all spins were complete, the furnace was powered off and all interior components were allowed to cool.

Chapter 2 References:

[1] Victrex plc. Victrex 150G Datasheet, Victrex Plc, July 2017.

[2] Victrex plc. Victrex 450G Datasheet, Victrex Plc, July 2017.

[3] Victrex plc. Victrex 650G Datasheet, Victrex Plc, July 2017.

[4] Dalton P, Grafahrend D, Klinkhammer K, Klee D, Möller M. Electrospinning of polymer melts: phenomenological observations, Polymer (2007), Volume 28, Pages 6823–33. Doi: 10.1021/bm050777q.

[5] Zhmayev E, Cho D, Joo YL. Modeling of melt electrospinning for semi-crystalline polymers, Polymer (2010), Volume 51, Issue 1, Pages 274-290. ISSN 0032-3861. Doi: 10.1016/j.polymer.2009.11.025.

[6] Ko J, Mohtaram NK, Ahmed F, Montgomery A, Carlson M, Lee PC, Willerth SM, Jun MBG. Fabrication of poly (ϵ-caprolactone) microfiber scaffolds with varying topography and mechanical properties for stem cell-based tissue engineering applications, Journal of Biomaterials Science: Polymer Edition (2013), Volume 25, Issue 1, Pages 1-17. Doi: 10.1080/09205063.2013.830913.

[7] Zhou H, Green TB, Joo YL. The thermal effects on electrospinning of polylactic acid melts, Polymer (2006), Volume 47, Pages 7497–7505. Doi: 10.1016/j.polymer.2006.08.042.

[8] Lyons J, Li C, Ko F. Melt-electrospinning part I: processing parameters and geometric properties, Polymer (2004), Volume 45, Issue 22, Pages 7597-7603. ISSN 0032-3861. Doi: 10.1016/j.polymer.2004.08.071.

[9] 3M Company. 3M Polyimide Film Tape 5413 Datasheet, 3M Company, September 2014.

[10] Allen NL. Chapter – 20, Fundamental aspects of air breakdown, 'High Voltage Engineering and Testing', Energy Engineering (2001), 2nd ed., IET Digital Library, Pages 581-600. Doi: 10.1049/PBPO032E_ch20.

[11] DuPont. DuPont Kapton Summary of Properties, Dupont. January 2017.

[12] Lugo LM, On the inertia and generalization of Coulomb's law, Physics Essays (2011), Volume 24, Issue 3, Pages 345-348. Doi: 10.4006/1.3598139.

[13] Kong CS, Jo KJ, Jo NK, Kim HS. Effects of the spin line temperature profile and melt index of poly(propylene) on melt-electrospinning, Polymer Engineering Science (2009), Volume 49, Pages 391–396. Doi: 10.1002/pen.21303.

[14] Fang J, Zhang L, Sutton D, Wang X, Lin T. Needleless melt-electrospinning of polypropylene nanofibres, Journal of Nanomaterials (2012), Volume 2012, Pages 1-9. Doi: 10.1155/2012/382639.

Chapter 3 – Results

3.1 – Overview

As stated in Section 1.5, there are several established methods for analyzing fibers produced by electrospinning. This chapter will cover four types of analyses: SEM, TGA, FTIR, and POM. These will be used to evaluate the shape, quality, quantity, and thermal behavior of the electrospun PEEK fibers, as well as to evaluate some properties of crystalline structure within the fibers. By understanding the underlying properties of the PEEK fibers, it will be possible to assess the quality of the method presented in this thesis and the application potential of the PEEK fibers.

3.2 – SEM Results

A total of 11 samples were successfully electrospun, sputter coated with Gold-Palladium, and imaged by Nelaka Govinna using the Zeiss scanning electron microscope (Carl Zeiss Microscopy GmbH, Jena, Germany) located at 200 Boston Ave. Tufts University. These samples were produced using a variety of spin conditions so that the effects of applied voltage and working distance on the fiber diameter and quality could be analyzed. First in this section, the overall fiber orientation of the eleven samples made with six different spin conditions will be presented (see Figures 3.1-3.11). Second, the measured fiber diameters will be presented. Third, some unique fiber characteristics will be shown in high detail.

3.2.1 – Fiber Orientation

The general fiber orientations resulting from six unique working conditions during electrospinning are shown below. Some working conditions were repeated more than once to see average behavior over several spins and eliminate outlying behavior. Of the eleven

samples shown, some are shown on an Aluminum foil substrate characterized by striations, and the remaining samples are shown on a Pelco tab adhesive substrate (Ted Pella Inc., Redding, CA) characterized by a smooth bubbly appearance.

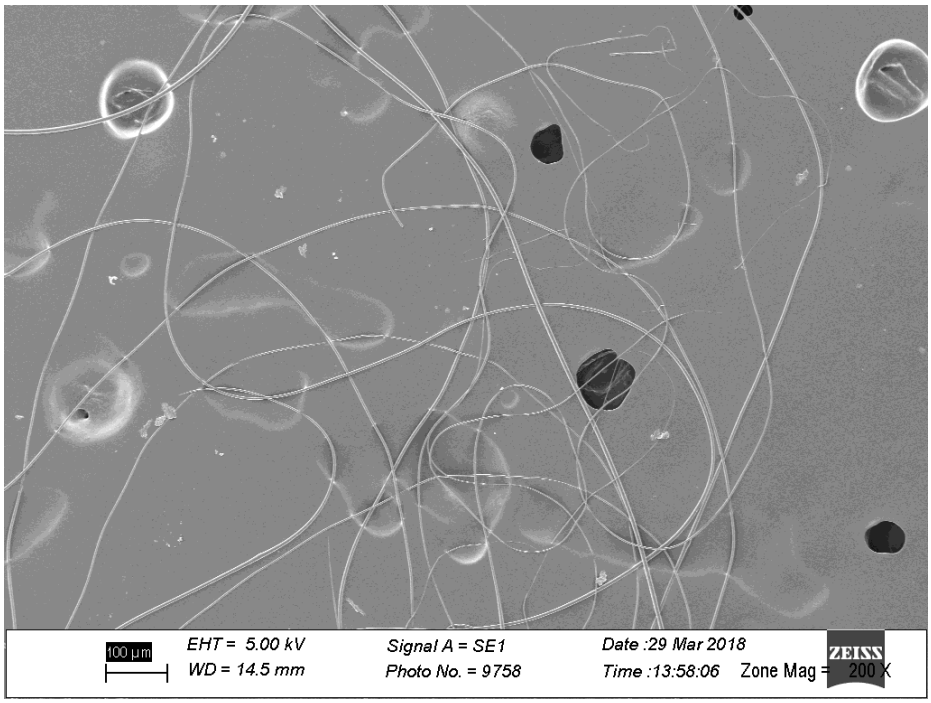

Figure 3.1: SEM Image of sample 1 spun at an applied voltage of 7.5 kV and a working distance of 3.6 cm. The scale bar represents 100 microns.

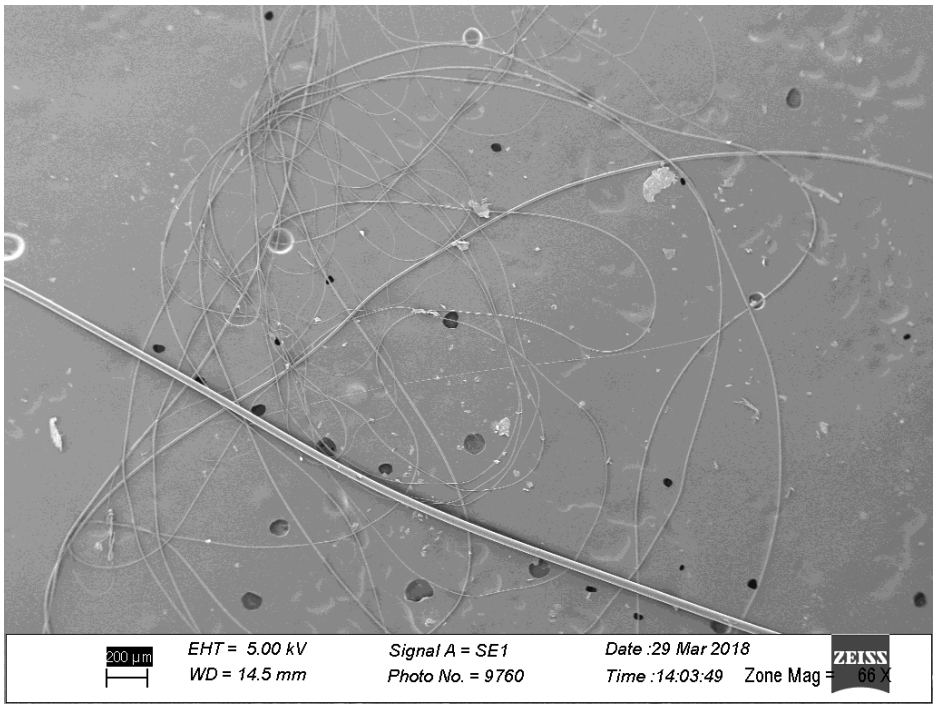

Figure 3.2: SEM Image of sample 2 spun at an applied voltage of 7.5 kV and a working distance of 3.6 cm. The scale bar represents 200 microns.

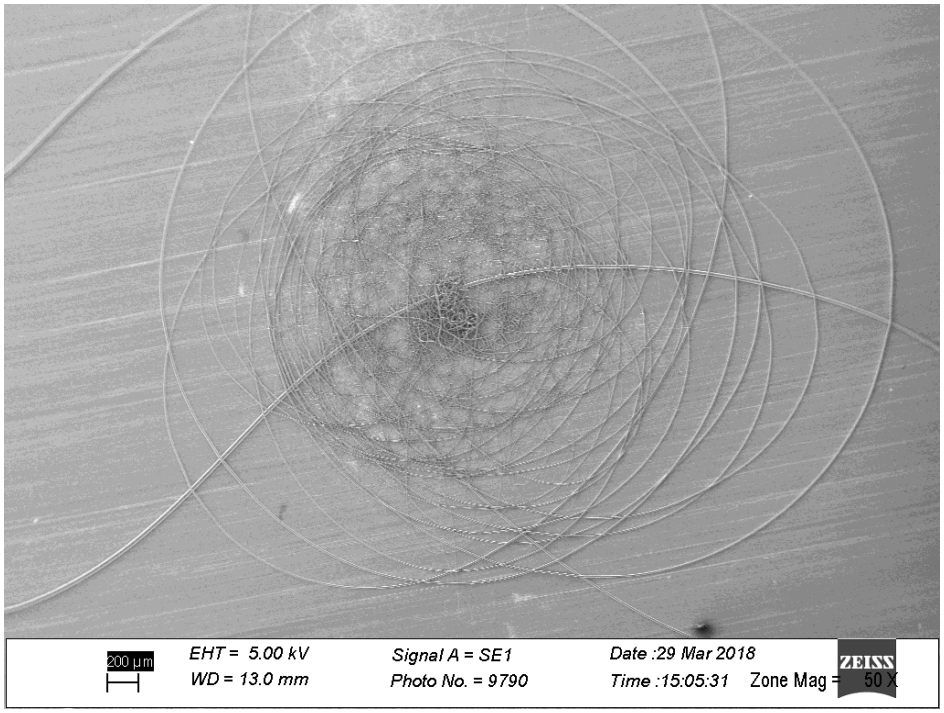

Figure 3.3: SEM Image of sample 3 spun at an applied voltage of 10 kV and a working distance of 3.6 cm. The scale bar represents 200 microns.

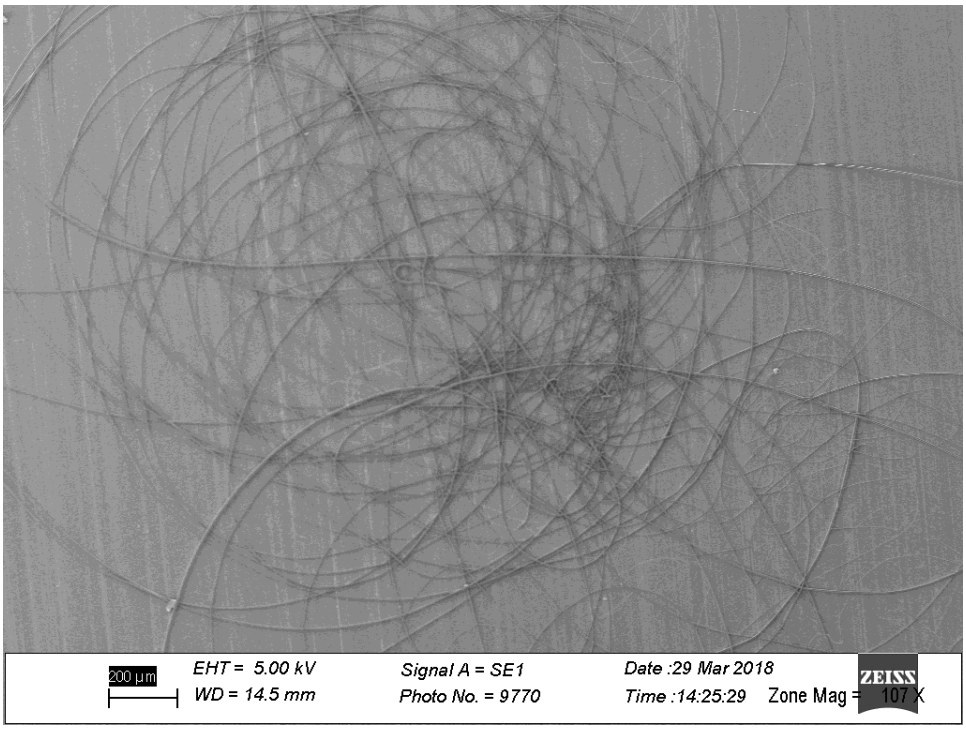

Figure 3.4: SEM Image of sample 4 spun at an applied voltage of 10 kV and a working distance of 3.6 cm. The scale bar represents 200 microns.

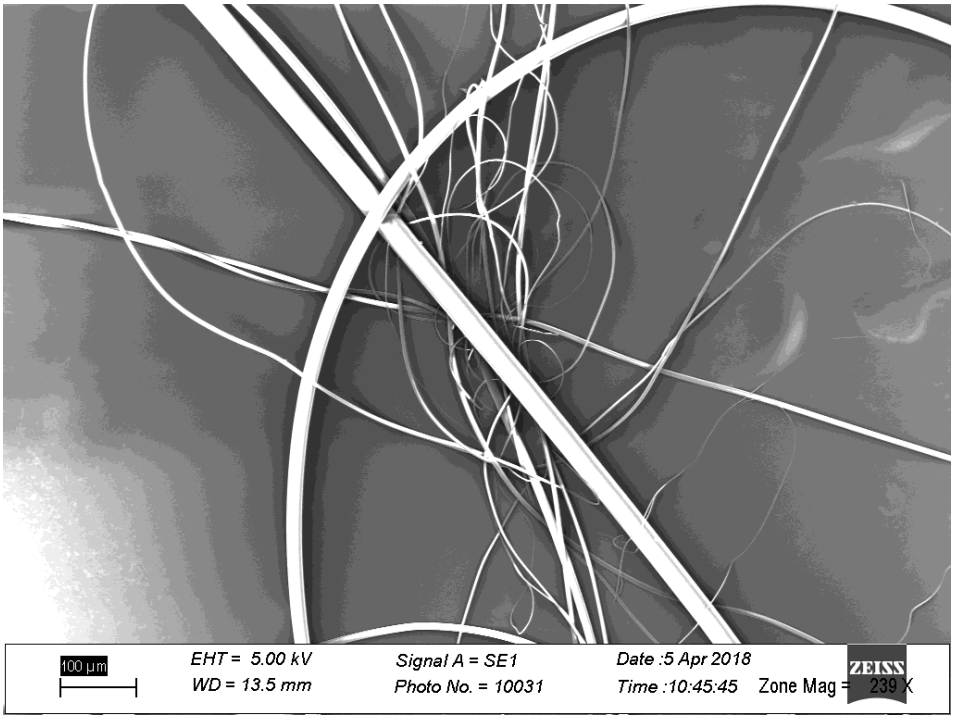

Figure 3.5: SEM Image of sample 5 spun at an applied voltage of 10 kV and a working distance of 3.6 cm. The scale bar represents 100 microns.

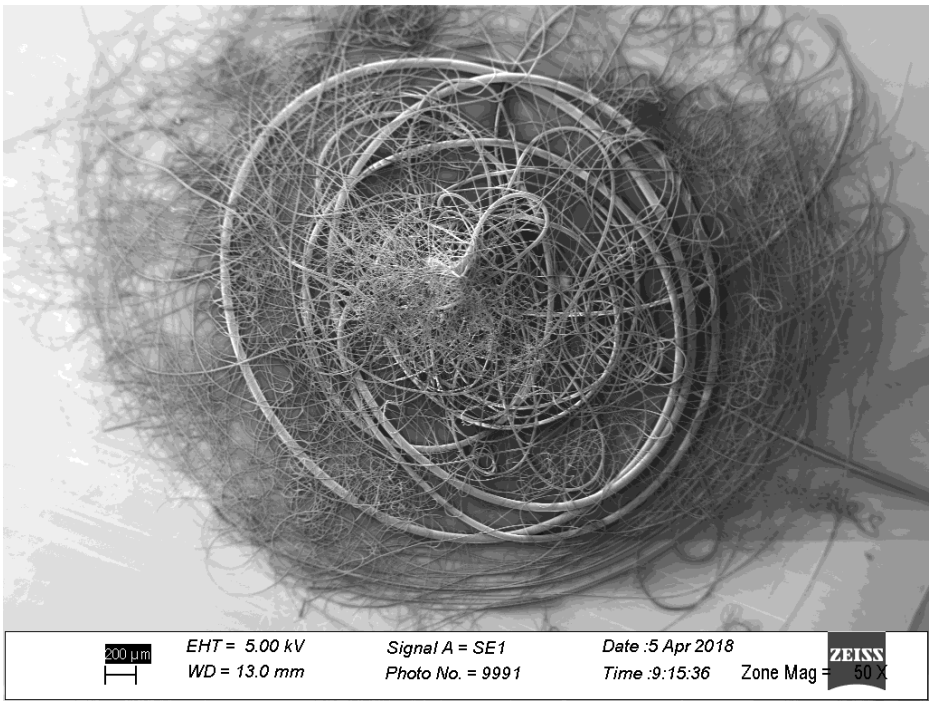

Figure 3.6: SEM Image of sample 6 spun at an applied voltage of 12.5 kV and a working distance of 3.8 cm. The scale bar represents 200 microns.

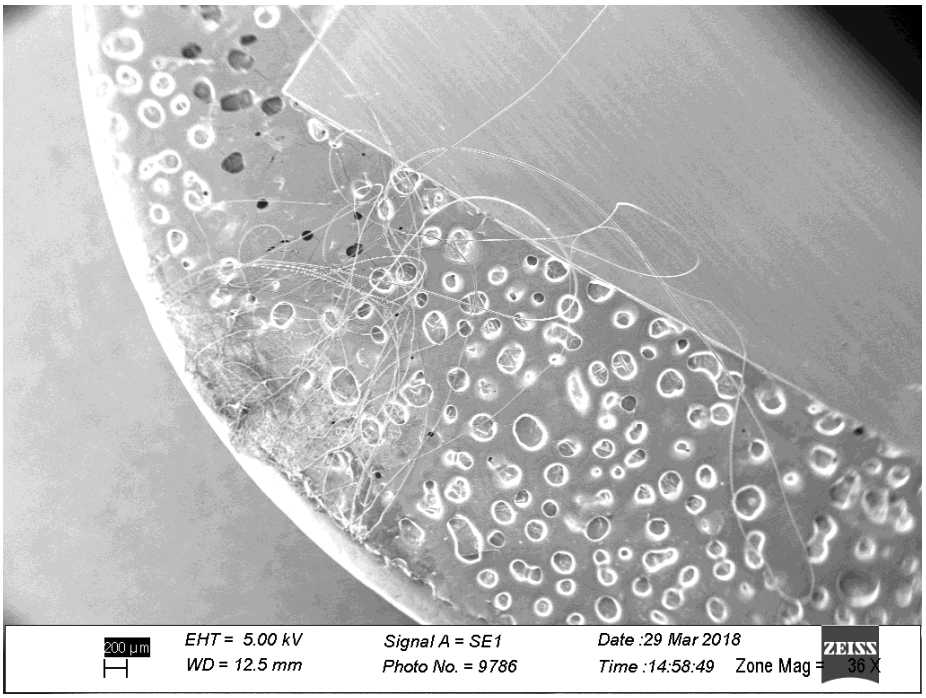

Figure 3.7: SEM Image of sample 7 spun at an applied voltage of 13 kV and a working distance of 3.6 cm. Note that this sample was blown off the Al substrate onto the Pelco tab during the sputtering process, so its orientation was altered. The scale bar represents 200 microns.

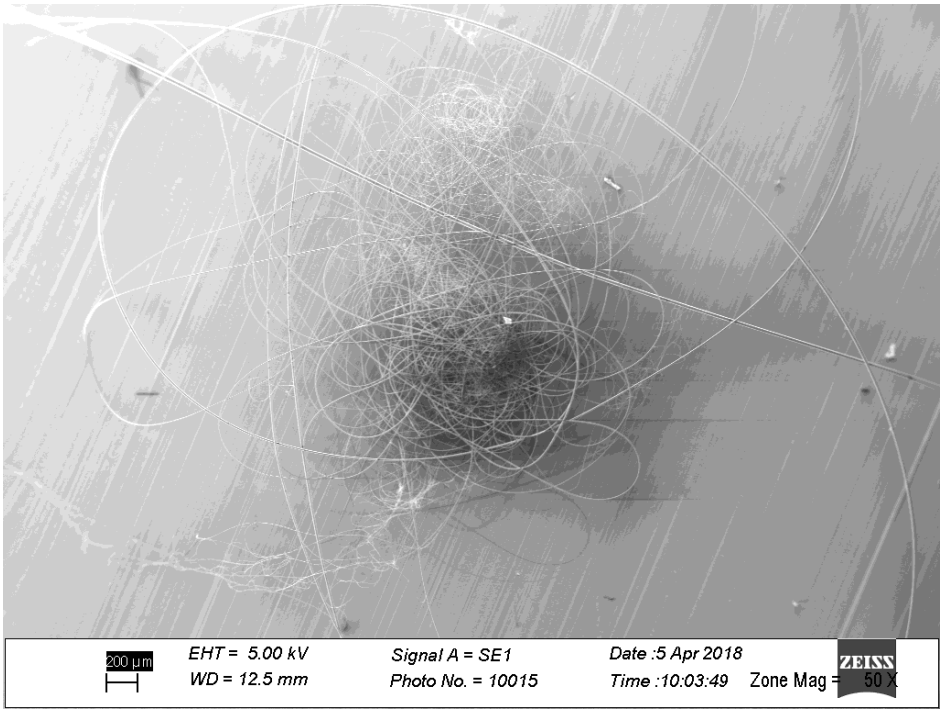

Figure 3.8: SEM Image of sample 8 spun at an applied voltage of 13 kV and a working distance of 3.6 cm. The scale bar represents 200 microns.

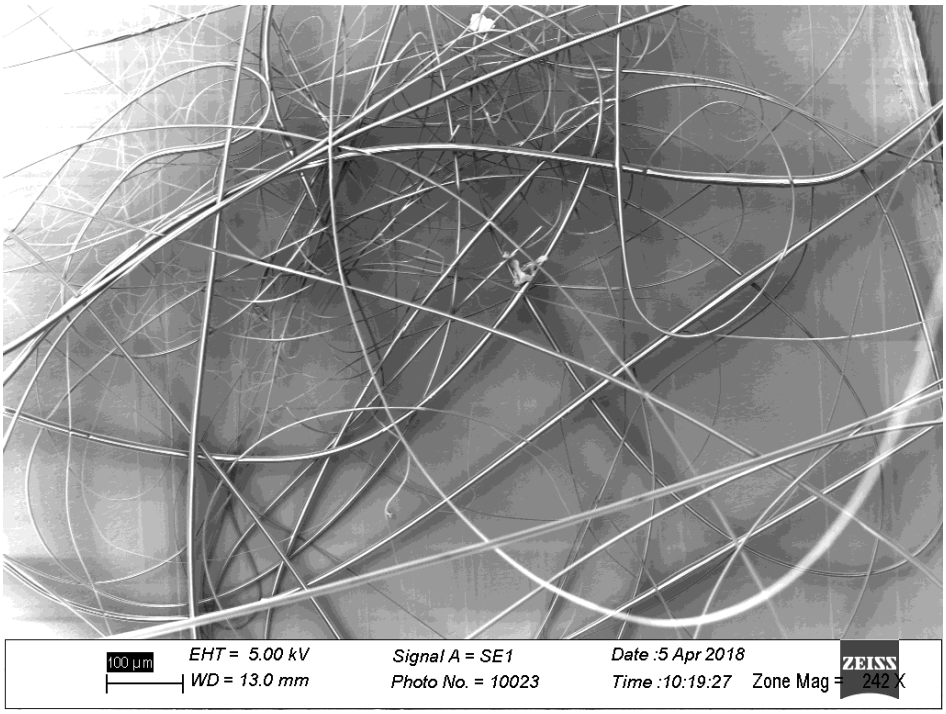

Figure 3.9: SEM Image of sample 9 spun at an applied voltage of 13 kV and a working distance of 3.6 cm. The scale bar represents 100 microns.

Figure 3.10: SEM Image of sample 10 spun at an applied voltage of 15.5 kV and a working distance of 3.8 cm. The scale bar represents 300 microns.

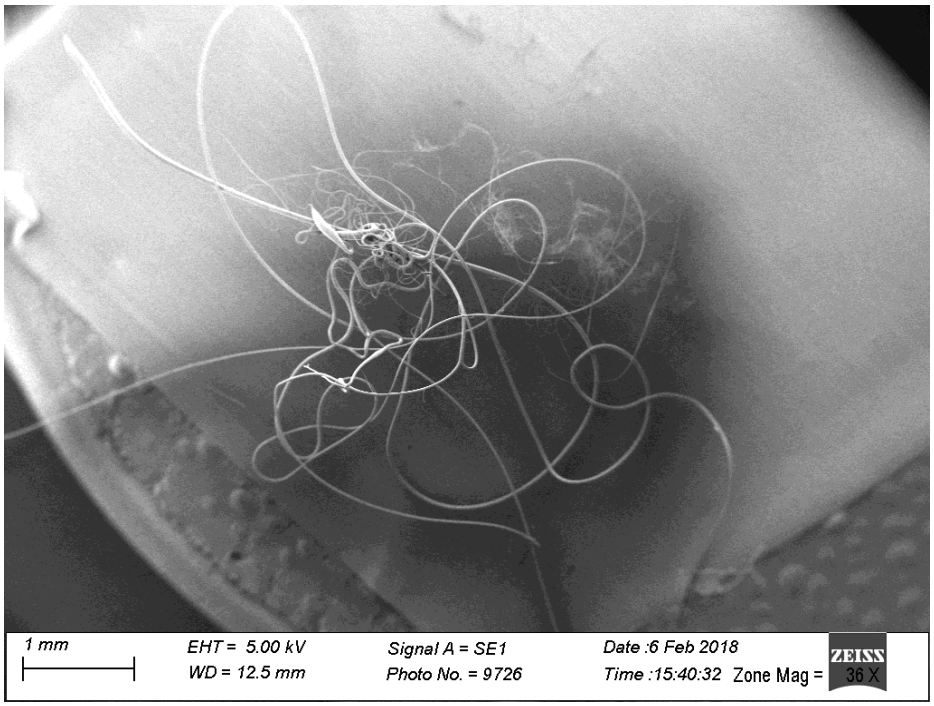

Figure 3.11: SEM Image of sample 11 spun at an applied voltage of 16 kV and a working distance of 3.6 cm. The scale bar represents 1 mm.

Some general remarks can be made about the fibers in Figures 3.7-3.12. First of all, each collection of fibers appears to be made of one continuous fiber. This correlates with a behavior seen while trying to remove the collector from the spinning area. If the fibers were still attached to the PEEK source droplet by an interstitial fiber and the collector was pulled away from the spinning area, the still attached fiber would sometimes pull the entire spun fiber mat off of the collector in one long continuous fiber.

Second, there certainly appears to be a correlation between fiber quantity and electric field strength. At too low an electric field strength, such as 2.78 kV/cm in Figures 3.1 and 3.2, there are very few fibers visible on the collector. This suggests that the electric field was too weak to sustain the electrospinning process for an extended period of time, and eventually the droplet simply fell off the spinneret without having many fibers drawn to the collector. However, at too high an electric field strength, such as 4.44 kV/cm in Figure 3.11, there are also few fibers visible on the collector. In this case though, the electric field strength was so high that the entire source droplet was pulled to the collector during the spinning process, halting the spin after a short period of time. Therefore, there seems to be a sweet spot for this method in between these two extremes, from 10-13 kV over 3.6-3.8 cm and from 12.5-15.5 kV over 3.8 cm, where the fibers are drawn off the spinneret at an appropriate rate to facilitate electrospinning over an extended period of time.

3.2.2 – Fiber Diameters

The fiber diameters for all 11 samples were analyzed by mouse clicks using ImageJ, an image analysis program. Several representative SEM images of each sample were chosen to show the general fiber morphology and size. Diameters were drawn across each of the fibers in the foreground of each representative SEM image and a histogram was formed of the resulting measurements. Table 3.1 below summarizes the results of this analysis.

Generally, the average fiber diameter of all the samples was in the range 1.7 to 8.4 microns, with some outliers as small as 0.4 microns and as large as 50 microns. Table 3.1 presents data that further backs up the observations made in section 3.3.1. Samples 1 and 2 had an electric field strength of 2.78 kV/cm (7.5 kV over 3.6 cm), and consequently they show very low fiber number, higher average diameter, and no sub-micron fibers. On the other hand, sample 11 had an electric field strength of 4.44 kV/cm (16 kV over 3.6 cm), and yet it showed a lower fiber number, higher average diameter, and very high standard deviation. These observations fortify the conclusion that at too low an electric field strength (samples 1 and 2), there is inadequate force acting on the fiber to draw it into a sub-micron diameter, and at too high an electric field strength (sample 11), the fiber diameter becomes unpredictable.

Table 3.1: Histograms of Fiber Diameters at Various Electric Field Strengths

#	kV/cm	Av. Dia. (Micron)	St. Dev.	Fiber Number	Histogram
1	7.5/3.6	**5.6**	2.5	**43**	
*	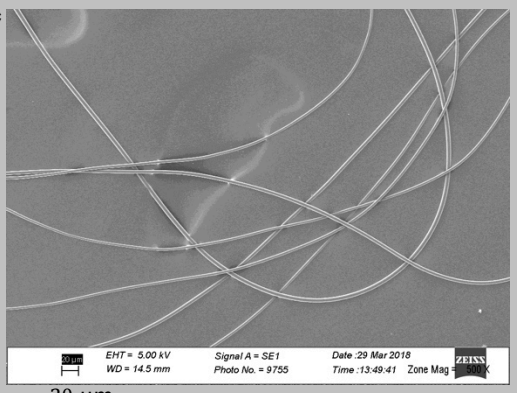 20 µm				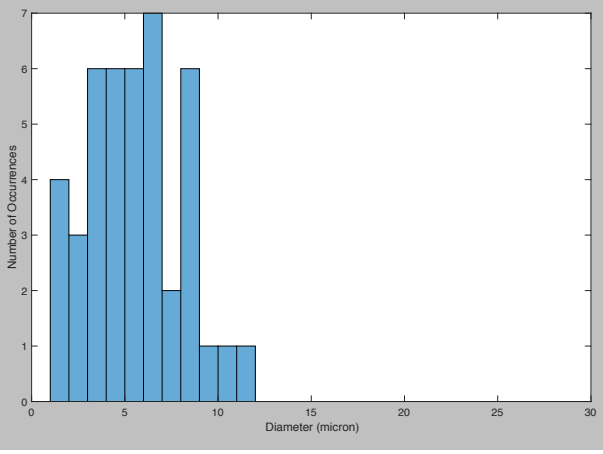
2	7.5/3.6	**6.4**	5.3	**58**	
	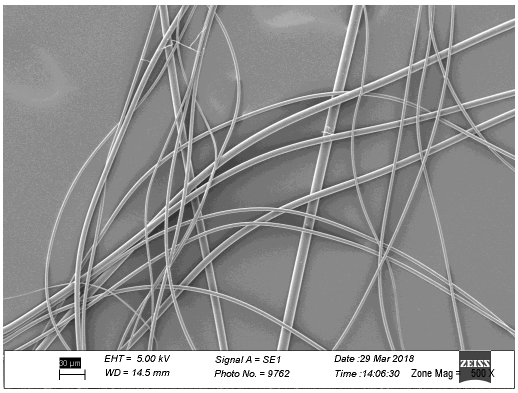 30 µm				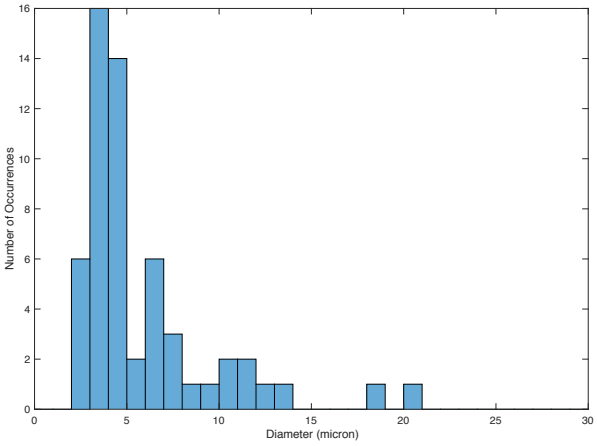
3	10/3.6	**3.4**	2.5	**169**	
	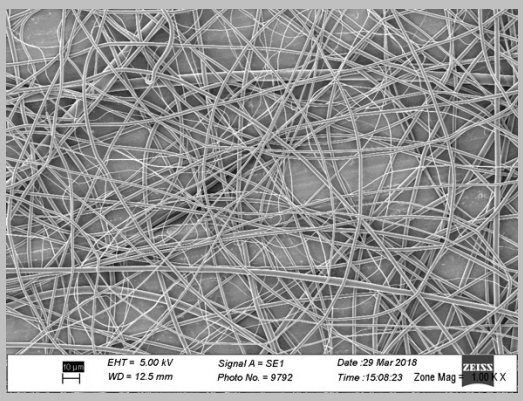 10 µm				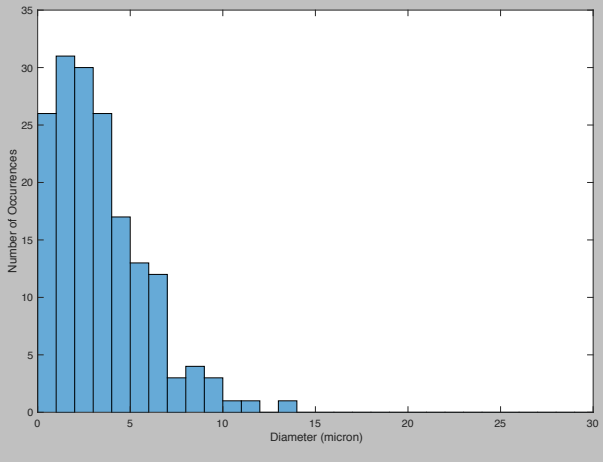

4 10/3.6 **3.4** 2.5 **208**

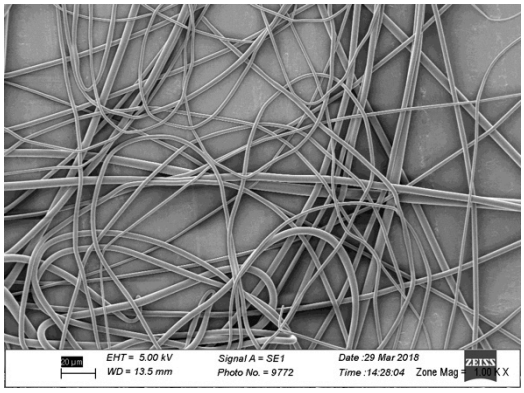

20 µm

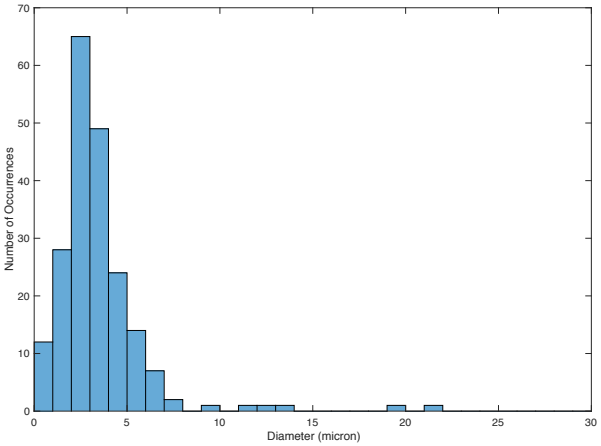

5 10/3.6 **8.4** 7.5 **65**

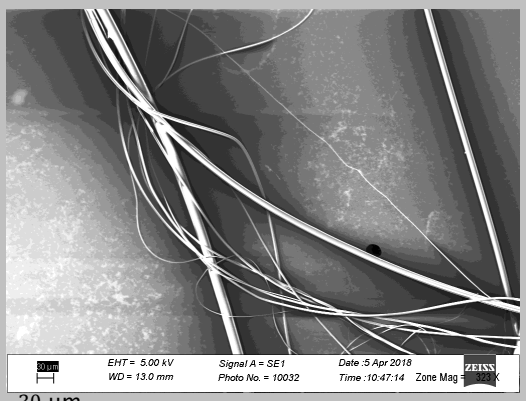

30 µm

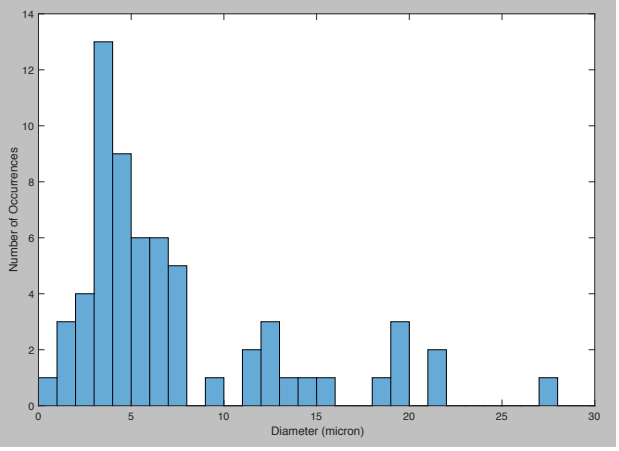

6 12.5/3.8 **4.5** 7.1 **260**

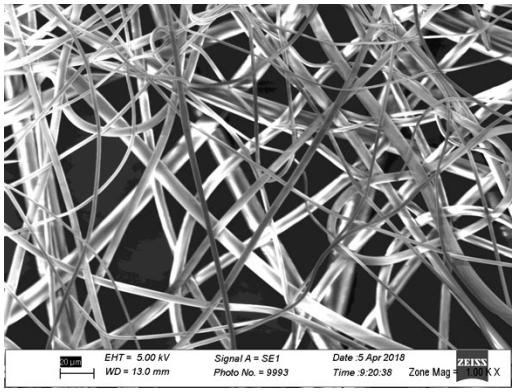

20 µm

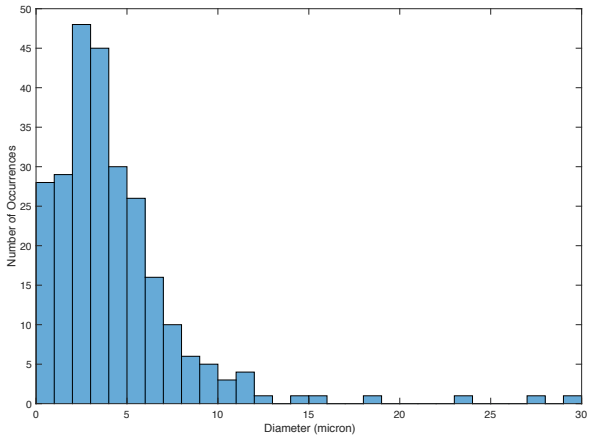

7 13/3.6 **3.9** 3.5 **224**

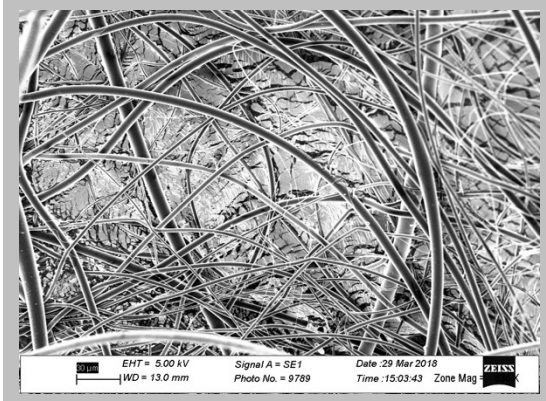

30 µm

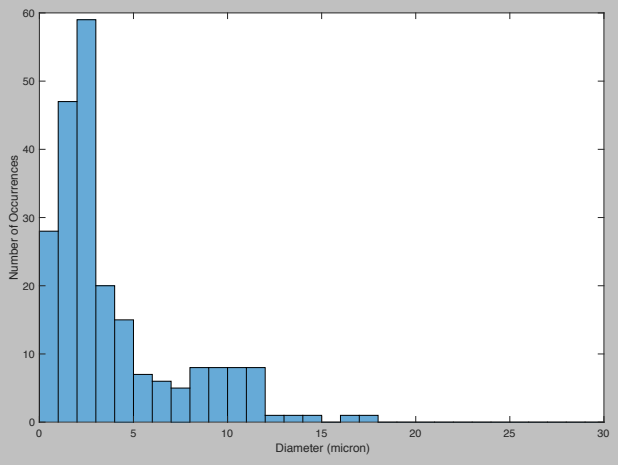

8 13/3.6 **2.8** 2.8 **229**

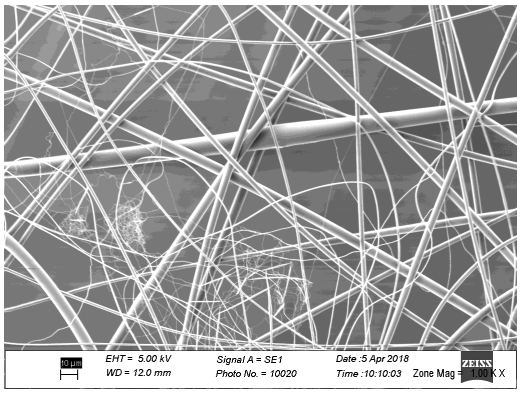

10 µm

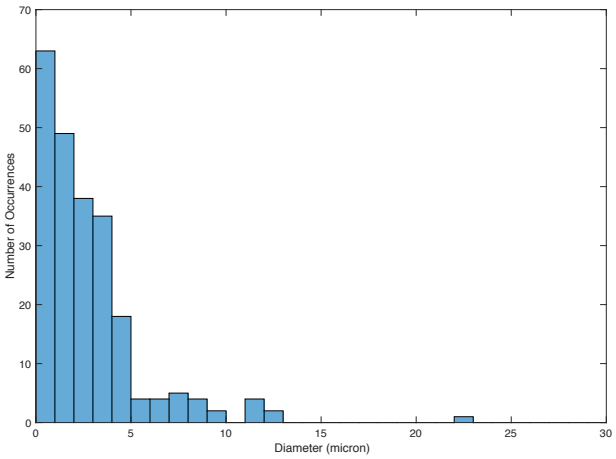

9 13/3.6 **1.7** 1.7 **104**

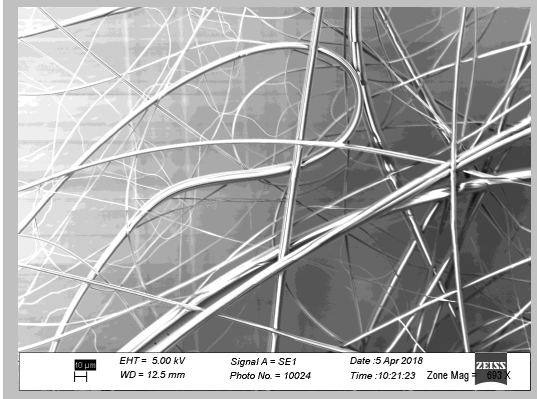

10 µm

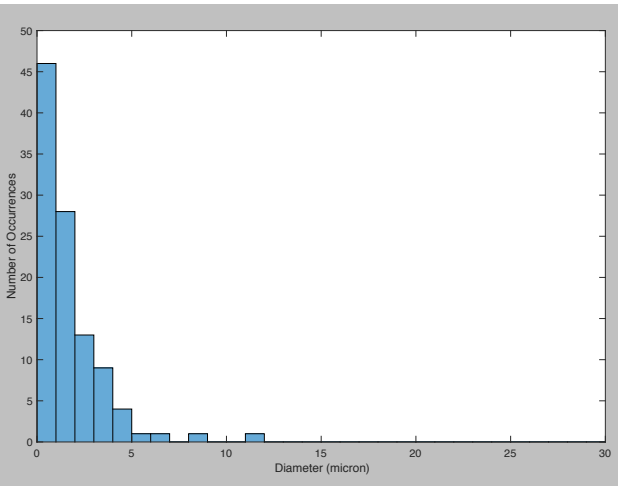

10	15.5/3.8	**3.6**	3.1	**258**

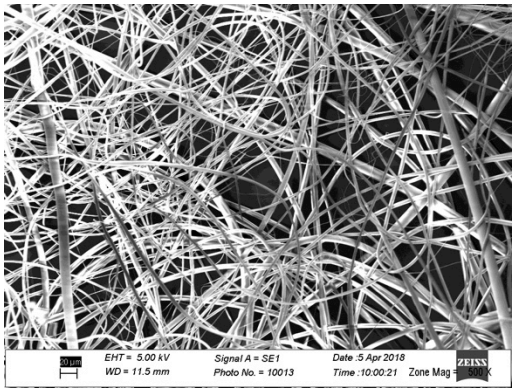

20 µm

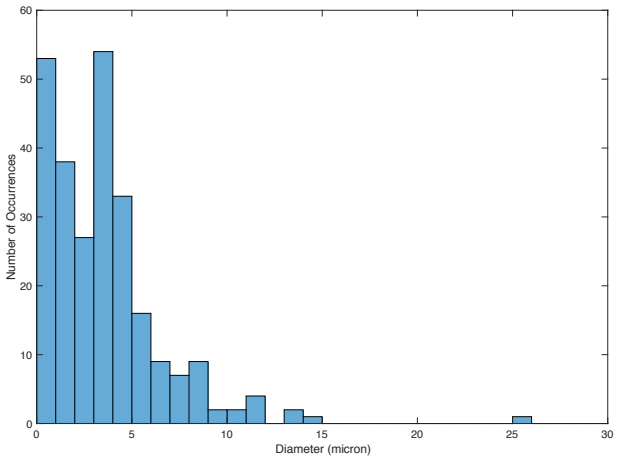

11	16/3.6	**5.8**	10.5	**153**

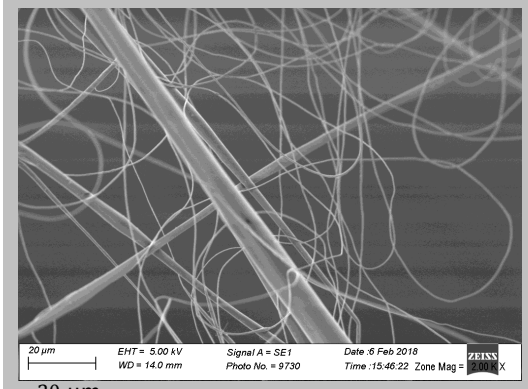

20 µm

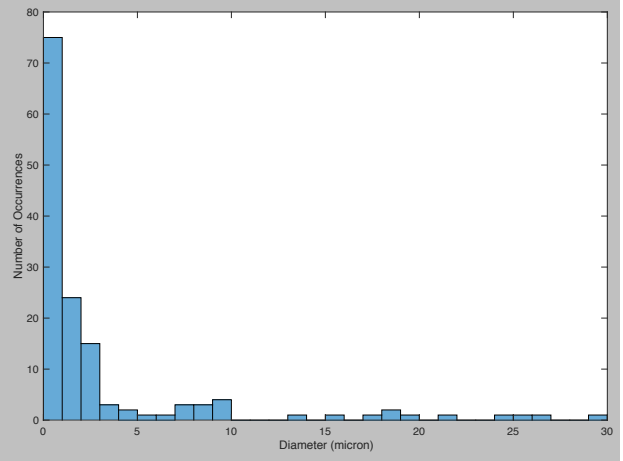

**Inset photos are representative images of the given sample of fibers. Four images of each sample were analyzed in addition to each representative image and the resulting data combined to form the histograms and averages.*

Clearly, the best fiber mats for having the smallest and most consistent diameters were those of samples 3-10, with some exceptions. For instance, sample 9 showed the lowest fiber diameter and standard deviation. However, this is misleading due to the fact that the fiber count is less than half the fiber counts of samples 7 and 8 under the same working conditions. While the average diameter of fibers in sample 9 was quite small (see Figure 3.12 and Table 3.1), they were spread out over the collector with few larger fibers in between; this resulted in very poor fiber density compared to samples 7 and 8.

Furthermore, sample 5 showed very low fiber number and large diameter compared to sample 4, under the same working conditions, and compared to the trend presented by the rest of the samples. Therefore, samples 5 and 9 should be taken as outliers within this data set. Sample 6 shows a high standard deviation in fiber diameter, but given its high fiber count and uniform overall morphology (see Figure 3.6) it will be taken as characteristic of this working condition and not an outlier.

Overall, no clear working conditions are shown to be significantly superior to the others within the set of samples 3, 4, 7, 8, and 10. All showed an average fiber diameter of between 3 and 5 microns and a standard deviation of less than 3.5 microns.

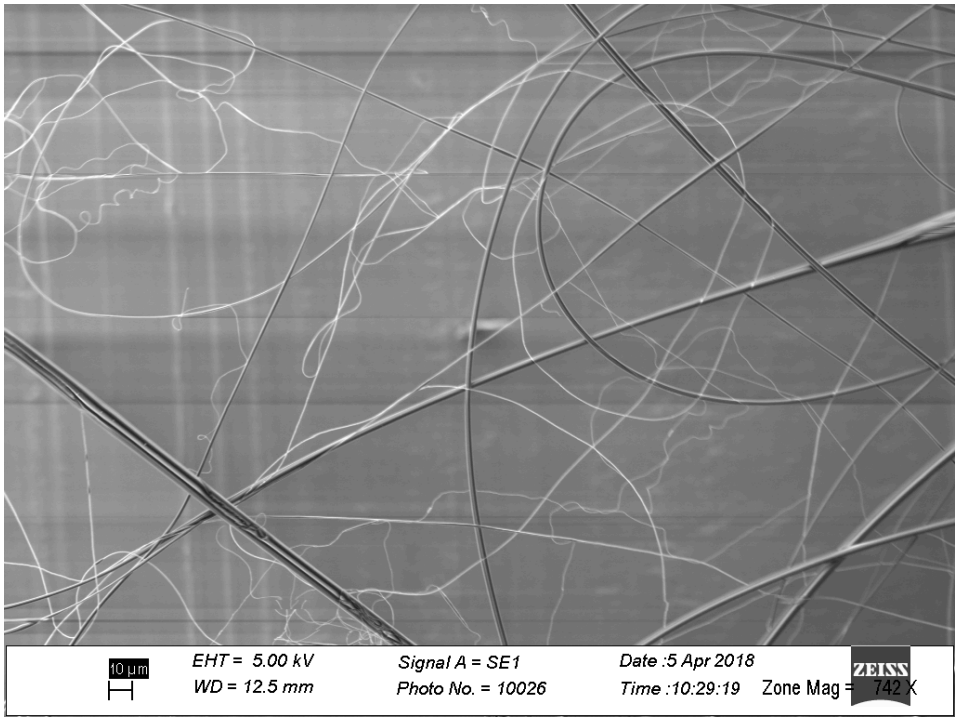

Figure 3.12: SEM Image of sample 9. Note the very small diameter fibers but low fiber density. The scale bar represents 10 microns.

3.2.3 – Unique Characteristics

The PEEK fibers produced using this method showed some unusual characteristics. First, it was common for sub-micron diameter fibers to be interspersed among much larger fibers. This occurred for all electric field strengths tested. For example, as shown in Figure 3.13, fibers of uniform diameter sometimes suddenly tapered down to a much smaller diameter, and then resumed their larger diameter after some distance along the fiber.

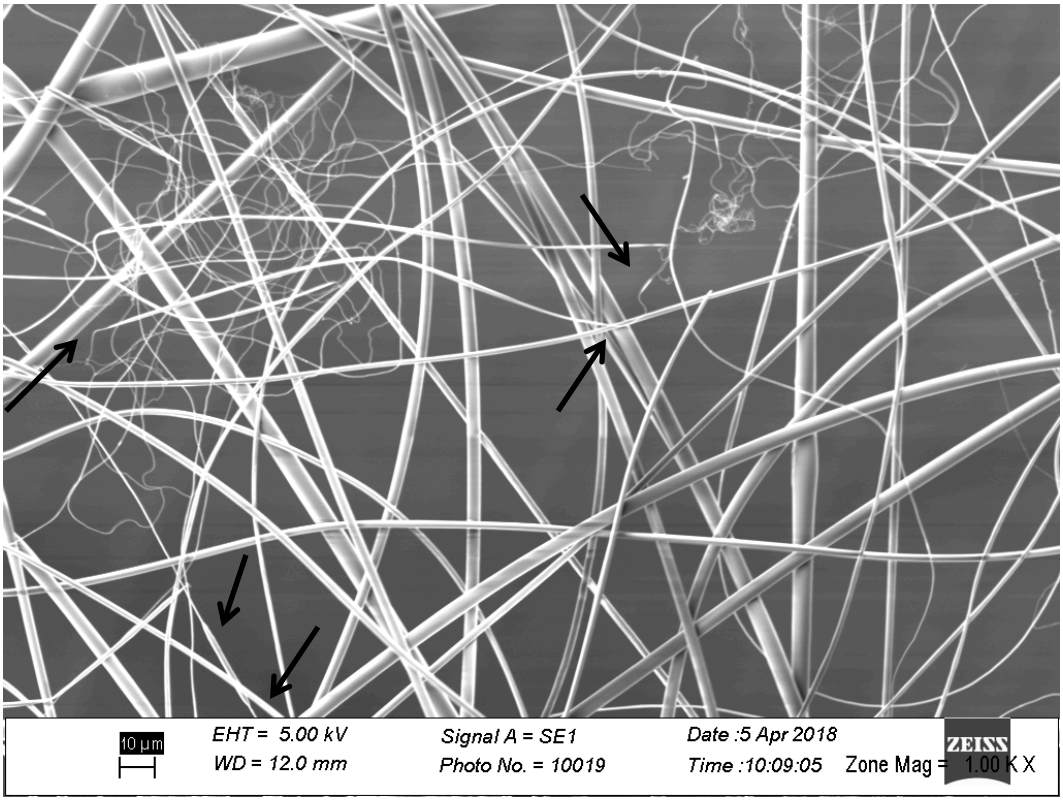

Figure 3.13: SEM Image of PEEK fibers on Sample 8, spun at an applied voltage of 13kV and a working distance of 3.6cm. The arrows indicate areas of sudden tapering or widening of the fibers. The scale bar represents 10 microns.

Similar behavior, known as "beading" has been thoroughly researched in solution electrospinning and can be caused by a number of factors including polymer viscosity, driving voltage, and flow rate from the spinneret [1]. However, as shown in Figure 3.14, the

"beads" formed during solution electrospinning are large, causing sudden increases in diameter along an otherwise uniform smaller diameter fiber. The fibers in Figure 3.13 exhibit behavior more resembling the sudden stretching of the fiber down to a small diameter between segments of larger diameter fiber. While the exact cause of this cannot be stated without directly observing the spin line and noting sudden decreases in fiber diameter, one suggestion can be made as to its cause. As stated in Sections 1.3 and 2.2, the temperature gradient of the spin line controls how long the polymer stays in a molten state and how long it can be subjected to the stretching forces in the spin line before beginning to crystallize and form a solid. The temperature of the spin line in this method was known to be difficult to control due to the turbulent mixing of hot furnace air with ambient air at room temperature. Therefore, during short instances where the spin line temperature varied to a higher value, it is possible that the polymer jet experienced a longer period of stretching and formed the small fibers seen in Figure 3.13. Then when the temperature varied lower, the polymer jet experienced a shorter stretching period and formed the other, larger fibers. However, this may be only a partial explanation for this phenomenon.

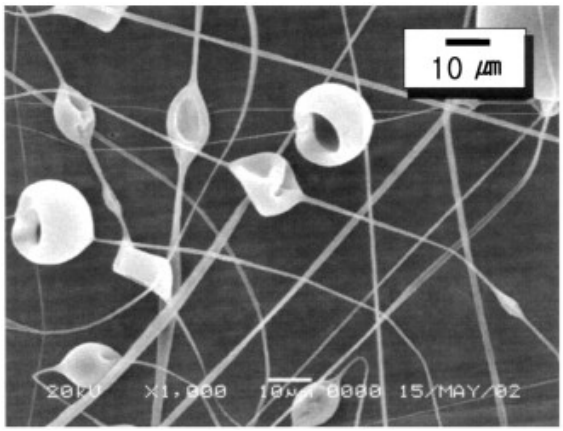

Figure 3.14: SEM Image of Polystyrene fibers with beads. The fibers were solvent electrospun at 13 percent concentration by weight in Tetrahydrofuran over a 12 cm working distance at 15 kV. Image from [2].

Second, collections of fibers often showed a circular or complex looping fiber orientation. This circular behavior can clearly be seen in Figures 3.8, 3.4, 3.6, and 3.8, where the fibers tended to coil up in a large spiral. Known as Liquid Rope Coiling, this effect is common in viscous fluids in the presence of a parallel force vector field, such as gravity or the electrostatic force from the collector, when they suddenly encounter a rigid surface [3]. The fluid assumes a direction of rotation and forms a corkscrew shape of fairly uniform radius as it piles up on top of itself.

However, in some instances, instead of a round circular shape a collection of recurring loops was seen, such as in Figure 3.15. Chiu-Webster, *et al.* [4] reported observing this phenomenon in research done analyzing a viscous thread of oil falling onto a surface. They observed that under static conditions, the thread tended to follow the model of the Liquid Rope. Yet when the surface was replaced with a belt moving at a relatively slow speed, this thread formed repeated loops of various sizes and increasing complexity as the belt speed was decreased. Therefore, adapting this model with the polymer fiber as the viscous thread, it can be inferred that the spin-line jet moving across the collector caused the regions of repeated looping. This makes sense, because the looping regions typically occurred at the edges of the fiber mat, where the jet appeared to wander off for a moment before returning the center of the fiber mat. The jet likely wandered due to instabilities in the spin-line caused by the turbulent convection currents of air interacting with the very delicate polymer jet.

This conclusion is supported by the work of Brown, *et al.* [5] researching direct writing of electrospun Polycaprolactone (PCL) fibers. They observed a similar behavior as they varied the speed of their moving collector; the fibers went from a straight line and gradually developed loops of increasing complexity as the speed of the collector was decreased (see Figure 3.16). Therefore, it seems important to note this behavior for

potential applications of electrospinning PEEK with a moving collector. The orientation of the fibers in the mat will be affected by the speed of the collector's movement.

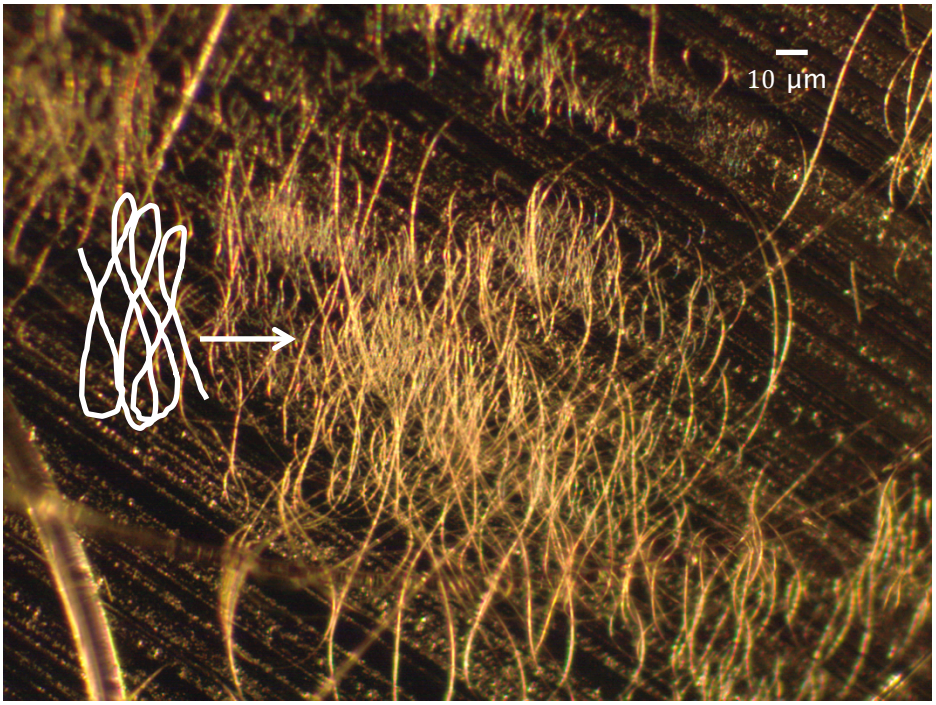

Figure 3.15: An optical image of electrospun PEEK fibers spun at 13 kV and 3.6 cm. Note the repeated looping of fibers as shown by the accompanying white outline. Image taken on a Nikon Eclipse E600 microscope with a SPOT Insight CCD camera under non-polarized illumination from an incident external light source on an aluminum foil substrate.

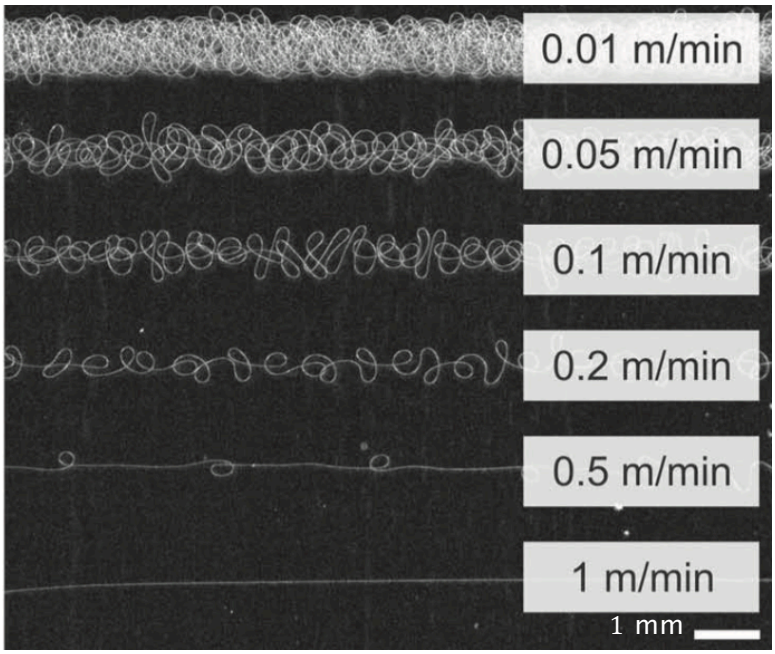

Figure 3.16: Optical image of melt electrospun PCL fibers spun at a 12 kV driving voltage and a 3 cm working distance. As the collector translation speed was decreased from 1.0 m/min to 0.01 m/ min, the complexity of the looping fibers increased. Image from [5].

Third, in only one specific fiber mat, sample 2, spherulites were visible on the surface of a large PEEK fiber, as shown in Figure 3.17. These chain-folded crystal structures radiate outward into the surrounding amorphous material from a nucleation site, and were only found on this one fiber among all the other fibers produced in this thesis. In order for polymer molecules to order themselves into a dense spherulitic crystal structure, a certain amount of time is required during cooling [6]. Upon full analysis of the situation, this fiber was an interstitial fiber, still attached to the spinneret after the spin was completed. This means that it remained mostly in the spin line and was not completely drawn to the collector. As a result, this fiber was allowed to cool slowly in the area of hot air just outside the furnace door, rather than cooling almost instantaneously like the fibers that reached the collector. Thus, the long amount of time allowed during cooling enabled these crystal structures to form. Close inspection shows that there is evidence of a puckered depression

in the center of the spherulites, possibly due to the contraction of the polymer as it formed dense crystal structures amid the surrounding lower density amorphous polymer. Nevertheless, this was an outlying case and was not typical of any other fibers studied in this thesis.

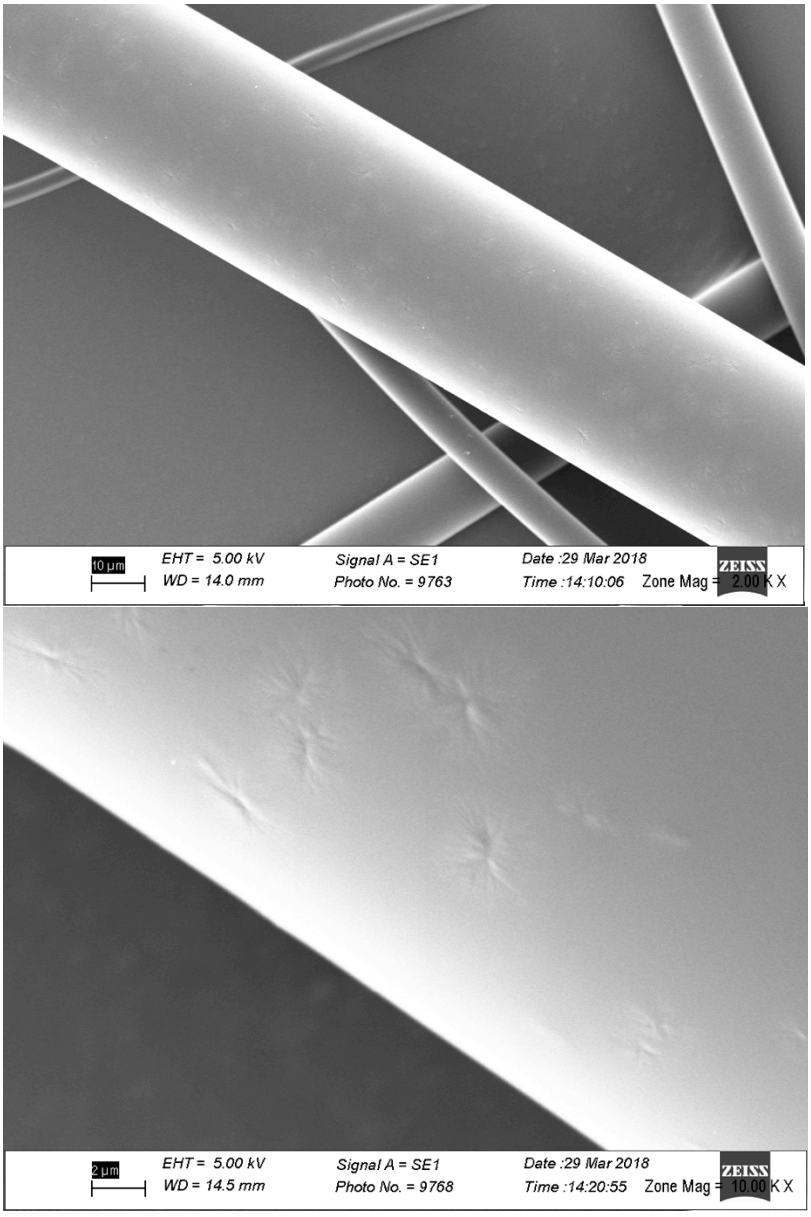

Figure 3.17: SEM image of the large interstitial fiber on sample 2 with visible spherulites on its surface at two magnification levels. The scale bar represents 10 and 2 microns respectively.

Fourth, the fibers were shown to pile up into a mound during spins where a large amount of fibers were produced such as in Figure 3.18. The mound has its peak at the center of the fiber mat and a smaller secondary hump corresponding to the area just below the center when the collector was horizontal. This makes sense because under the relatively symmetrical and parallel electrostatic force of attraction, the fibers are most likely to take the shortest path to the collector -within some deviation caused by whipping of the jet- and land in the area physically closest to the spinneret, the center of the mat, or just below this area if gravity significantly affects the trajectory of the fiber jet. This hypothesis is supported by the work of Dalton, *et al.* [7] who were able to directly observe the trajectory of the molten polymer jet of Polypropylene as it takes the shortest path to the collector, as shown in Figure 3.19.

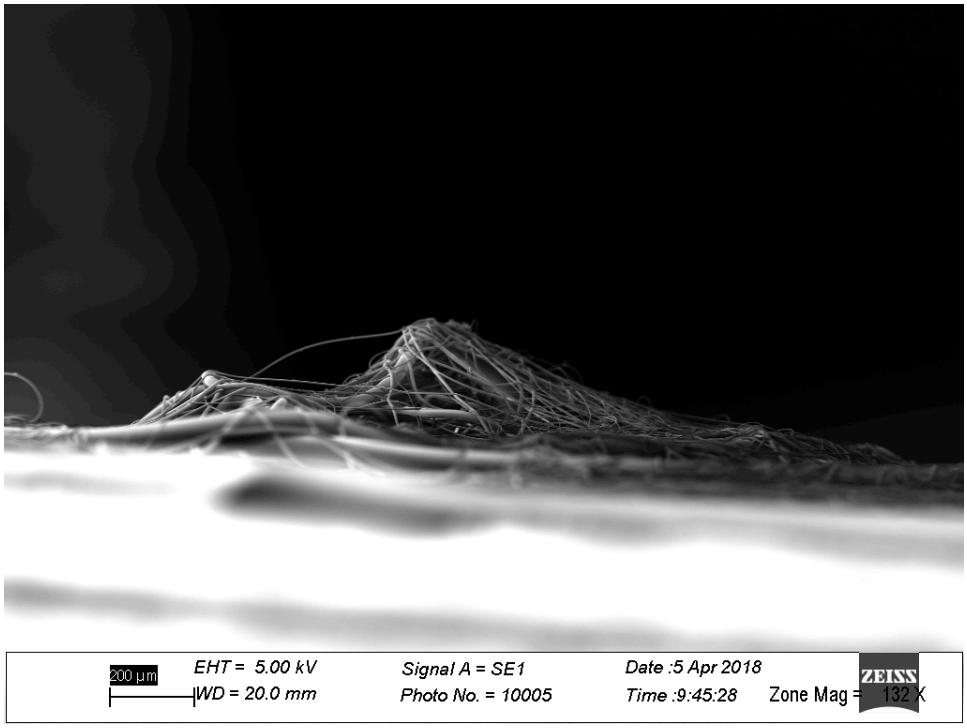

Figure 3.18: SEM image of the mound at the center of a fiber mat. This is the same sample shown in Figure 3.11 when viewed from the right, and was spun at 12.5 kV and 3.8 cm.

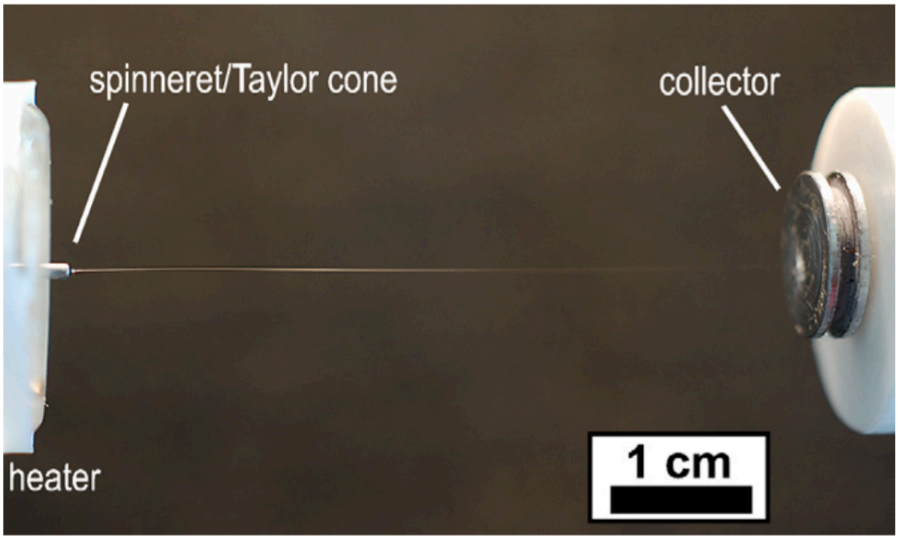

Figure 3.19: Photograph of a molten Polypropylene Taylor cone and jet as it travels from the spinneret to the Aluminum SEM stub collector in a fairly stable straight line, piling up in the center of the collector. Image from [7].

3.3 – TGA Results

TGA analysis was done to compare the thermal degradation behavior of the native PEEK pellets and the electrospun PEEK fibers with literature data on the behavior of S-PEEK. In theory, the PEEK fibers should show identical degradation behavior to the native PEEK pellets, since they are molecularly identical. TGA analysis was done in a Q500 Thermogravimetric Analyzer (TA Instruments, New Castle, DE) under a Nitrogen gas purge, ramping from 0 to 1000 °C at a rate of 20 °C per minute. Due to the extremely low mass of the fibers, a large droplet that had been drawn to the spinneret under the same working conditions as the fibers was substituted. Clearly, from Figures 3.20 and 3.21, the thermal behavior is roughly the same within a reasonable margin of experimental error. The PEEK droplet had a degradation temperature of roughly 596-598 °C, located where the derivative of weight with respect to time was at a maximum. This corresponds well to the literature value [8,9].

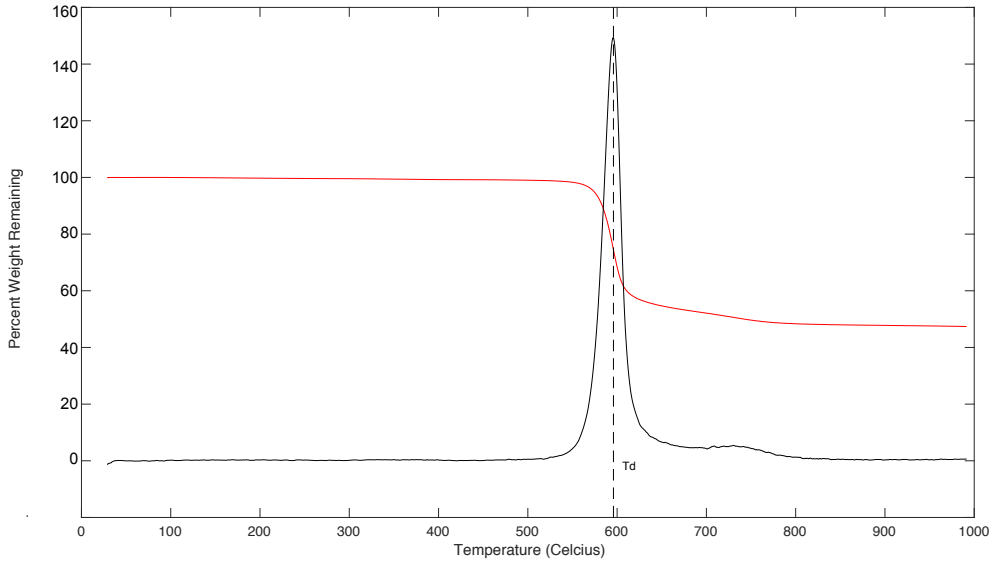

Figure 3.20: The weight remaining during heating at 20 °C/min for an electrospun PEEK droplet (red). The derivative of weight with respect to time (black) with its peak at 595.9 °C (dashed).

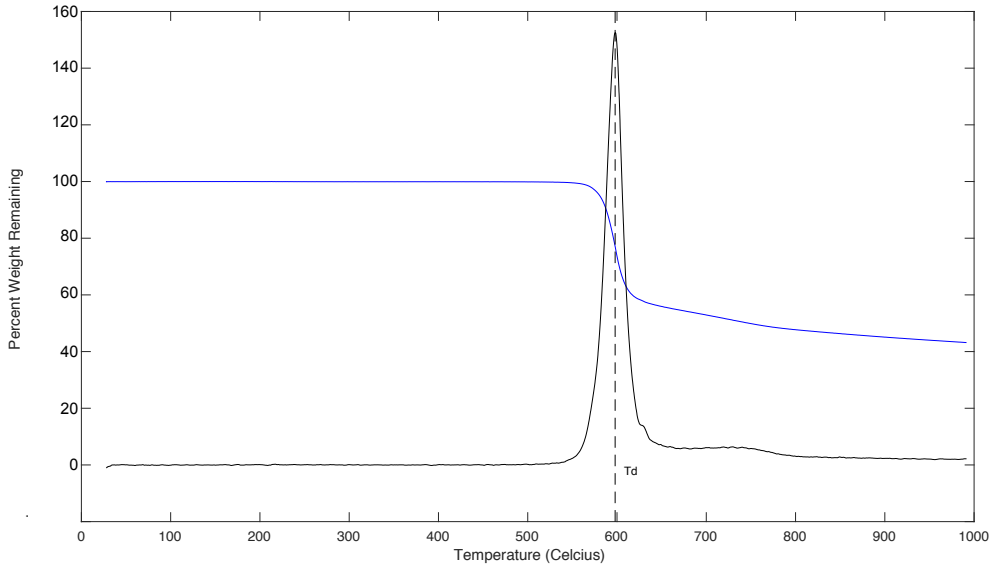

Figure 3.21: The weight remaining during heating at 20 °C/min for a native PEEK pellet (blue). The derivative of weight with respect to time (black) with its peak at 597.9 °C (dashed).

It is worth noting that in both the case of the droplet and the pellet, there was not complete mass loss at the end of this test. Rather, a small amount of char remained in the TGA basket, accounting for the residual mass. From Figures 3.20 and 3.21, the thermal characteristics of the electrospun PEEK fibers are shown to be essentially identical to those

of the native pellets. This serves as one clear source of evidence that these fibers are in fact PEEK and not from some unwanted source, such as S-PEEK shown in Figure 3.22.

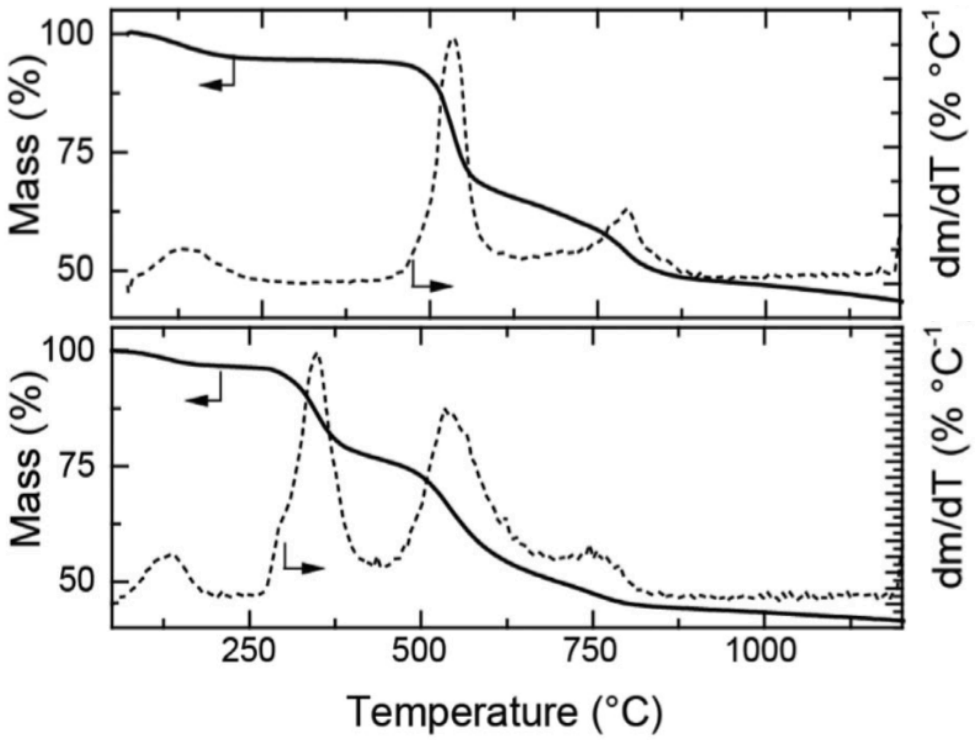

Figure 3.22: The weight remaining (thick black line) during heating at 20 °C/min for (top) N-S-PEEK film, (bottom) H-S-PEEK film. The derivative of weight with respect to time is shown as a dotted line in each plot, with the highest peak corresponding to the degradation temperature. Image from [9].

Finally as stated in Section 1.2, the degradation temperature of S-PEEK measured under the same heating rate of 20 °C/min is below 530 °C and sometimes as low as 345 °C depending on the counter-ion present. It is also worth noting that the water absorbance of S-PEEK is much higher than native PEEK. This was shown by the weight loss peak near 100 °C from water, as confirmed with mass spectrometry of the evaporated gas, for each form of

S-PEEK shown in Figure 3.22 [9]. The fibers produced in this thesis clearly possess thermal durability superior to S-PEEK fibers.

3.4 – FTIR Results

For the purposes of further confirming that the electrospun fibers are in fact PEEK, FTIR analysis was done on the native PEEK pellets and electrospun PEEK fibers. The FTIR analysis was done on a Jasco FT/IR-6200 (Jasco, Easton, MD) and analyzed using Jasco Spectra Manager software. Each sample had one scan performed from 650 cm^{-1} to 1800 cm^{-1} at 2 cm^{-1} resolution with an air background subtraction and were baseline corrected. This analysis makes it possible to compare the molecular structure of the PEEK fibers with the native PEEK pellets, as well as with literature FTIR data for sulfonated S-PEEK fibers. FTIR is useful for observing the interaction between infrared light and the molecules within a polymer. Each molecule and molecular group within a polymer has some degree of freedom with which it can rotate or vibrate within the molecular at large. Generally, these degrees of freedom can be excited by light in the infrared spectrum. Therefore, by bombarding the sample polymer with a broad spectrum of infrared light, the polymer selectively absorbs certain wavelengths corresponding to specific degrees of freedom of its component molecules. In this way, noting the specific peaks that characterize a polymer can make a general molecular and structural "fingerprint" [10].

The literature characteristic peaks for PEEK in its native state are shown as dotted vertical lines in Figure 3.23 and Figures 3.24-3.26. These are according to the findings by Sadrjahani, *et al.* [11]. They also report the characteristic peaks for the sodium counter-ion form of S-PEEK, shown in Figures 3.24-3.26 at two levels of sulfonation, so that a direct comparison and differentiation can be made between S-PEEK fibers and those produced in this thesis.

Table 3.2: Characteristic FTIR peaks for native PEEK

Characteristic Peak	Wavenumber (1/cm)	Vibration
1	**1650**	**Carbonyl Stretching**
2	**1600**	**Skeletal Ring Vibration**
3	**1490**	**Skeletal Ring Vibration**
4	**1408**	**Skeletal Ring Vibration**
5	**1309**	**(C-C=O-C) Group Bending**
6	**1280**	**Diphenyl Ether Group Stretching**
7	**1224**	**Aromatic Hydrogen In-Plane Motion**
8	**1187**	**Diphenyl Ether Group Stretching**
9	**1159**	**Aromatic Hydrogen In-Plane Motion**
10	**1010**	**Aromatic Hydrogen In-Plane Motion**
11	**928**	**Aromatic Hydrogen Bending**
12	**860**	**Aromatic Hydrogen Bending**
13	**840**	**Aromatic Hydrogen Bending**
14	**767**	**Aromatic Hydrogen Bending**

Characteristic Peaks from [11].

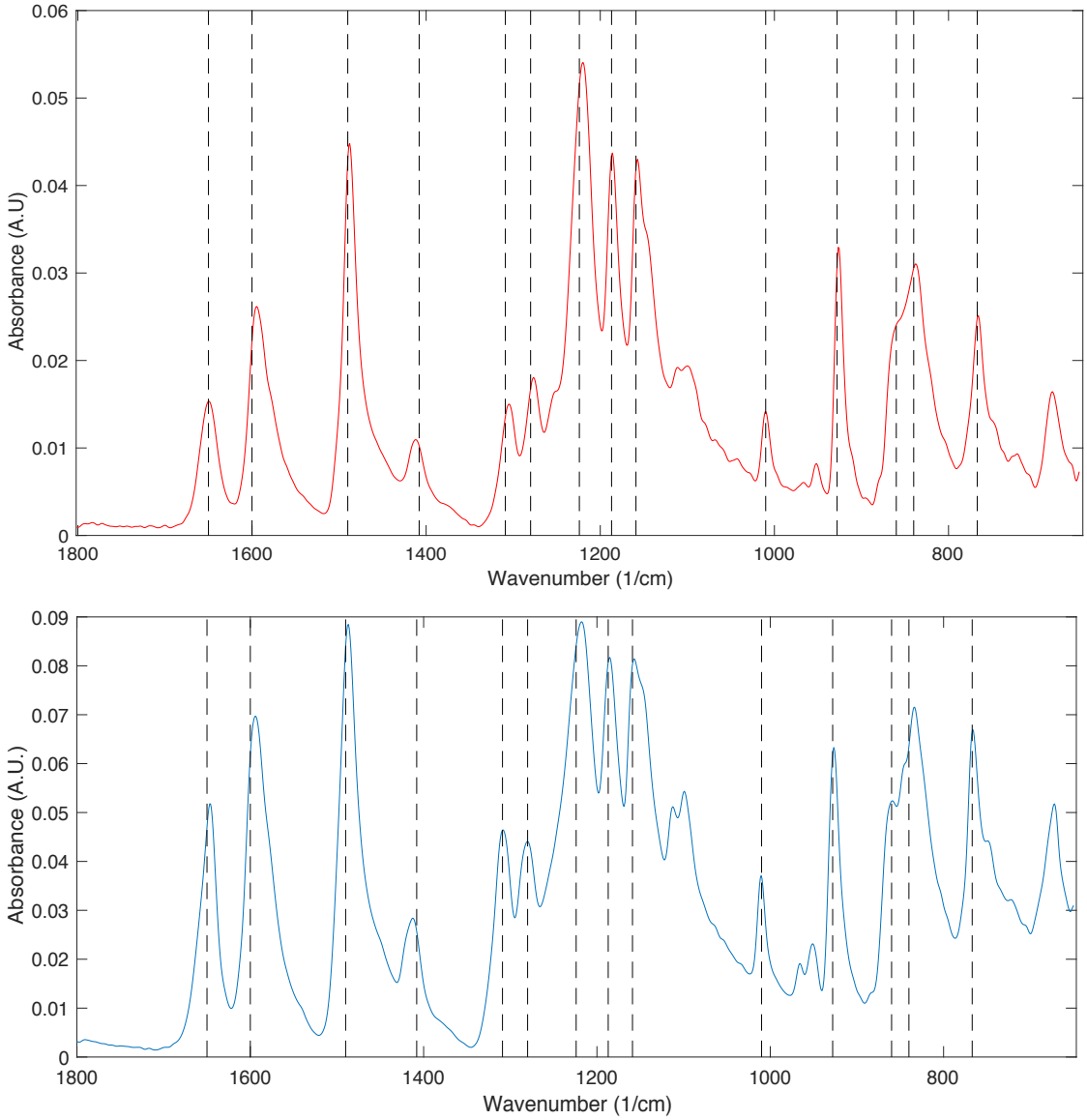

Figure 3.23: FTIR analyses of a native PEEK pellet as produced by the supplier (blue) and a mat of electrospun PEEK fibers (red) produced by this method. Note the characteristic peaks (dotted vertical lines) and their correspondence to the peaks shown in these graphs.

Comparing the native pellet and the electrospun fibers, it can clearly be seen that both figures show all the characteristic peaks of PEEK shown in Table 3.2. Some small deviations are visible between the two spectra at non-characteristic peaks, but these deviations are a result of different crystalline morphologies between the pellet and fibers,

which largely depend on the processing conditions by which each was formed and not necessarily from molecular differences. For example, since the fibers were formed from a native pellet, they are expected to have had identical crystal morphology to the pellet before the electrospinning process, assuming consistent manufacturing procedures on the part of the supplier. However, during the melt electrospinning of a similar polymer, Nylon, Joo, *et al.* [12] observed significant effects of flow-induced crystallization in the electrospun fibers, as the stresses inside the polymer jet cause large-scale polymer chain alignment along the axis of the fiber and rapid crystallization. Therefore, this flow-induced crystallization behavior likely explains some of the deviations in FTIR spectra between the pellet and fibers.

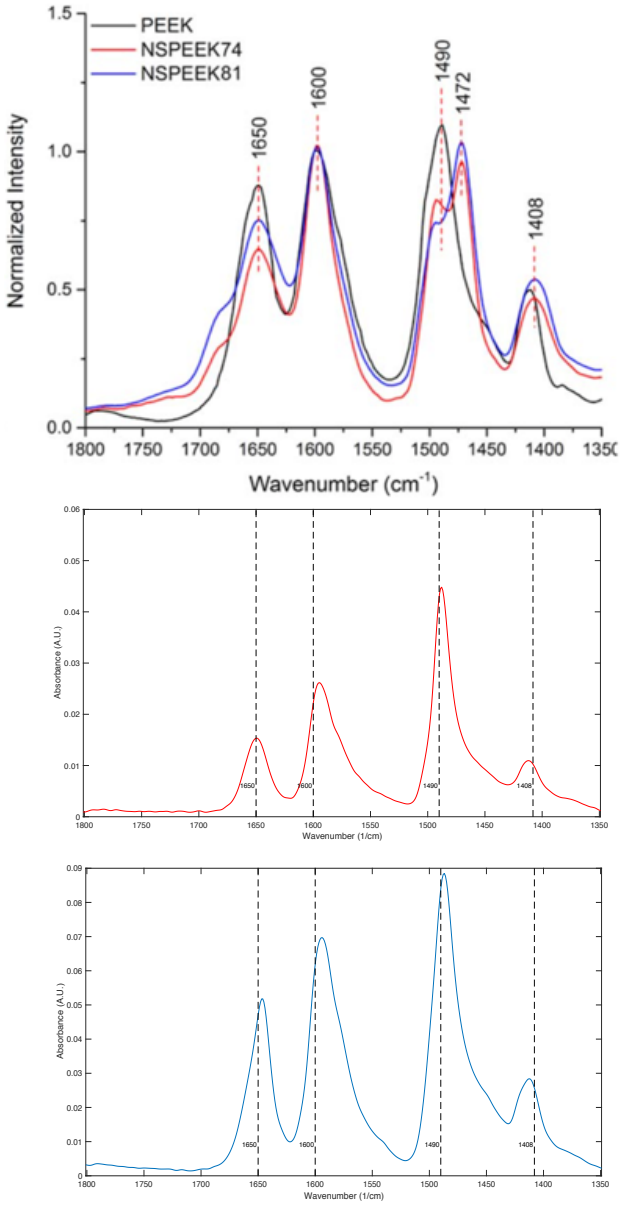

Figure 3.24: FTIR analyses of (top) PEEK and S-PEEK at two degrees of sulfonation, (middle) PEEK fibers, (bottom) the native PEEK pellet. Note the size of the 1472 peak increases and the size of the 1490 peak decreases with degree of sulfonation. This shows a characteristic spectrum for S-PEEK that is distinct from PEEK. Top image from [11].

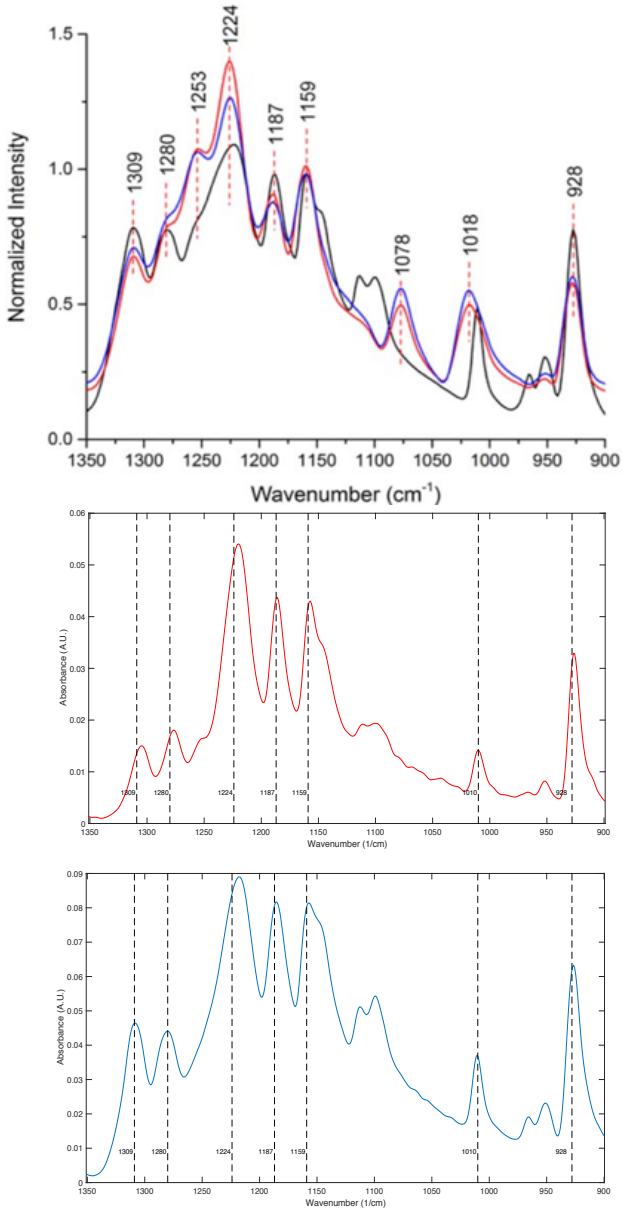

Figure 3.25: FTIR analyses of (top) PEEK and S-PEEK at two degrees of sulfonation, (middle) PEEK fibers, (bottom) native PEEK pellet. Note that the 1253 and 1078 peaks are only preset in S-PEEK. Also note the shift from 1010 to 1018 as sulfonation is increased. This further shows a characteristic spectrum for S-PEEK that is distinct from PEEK. Top image from [11].

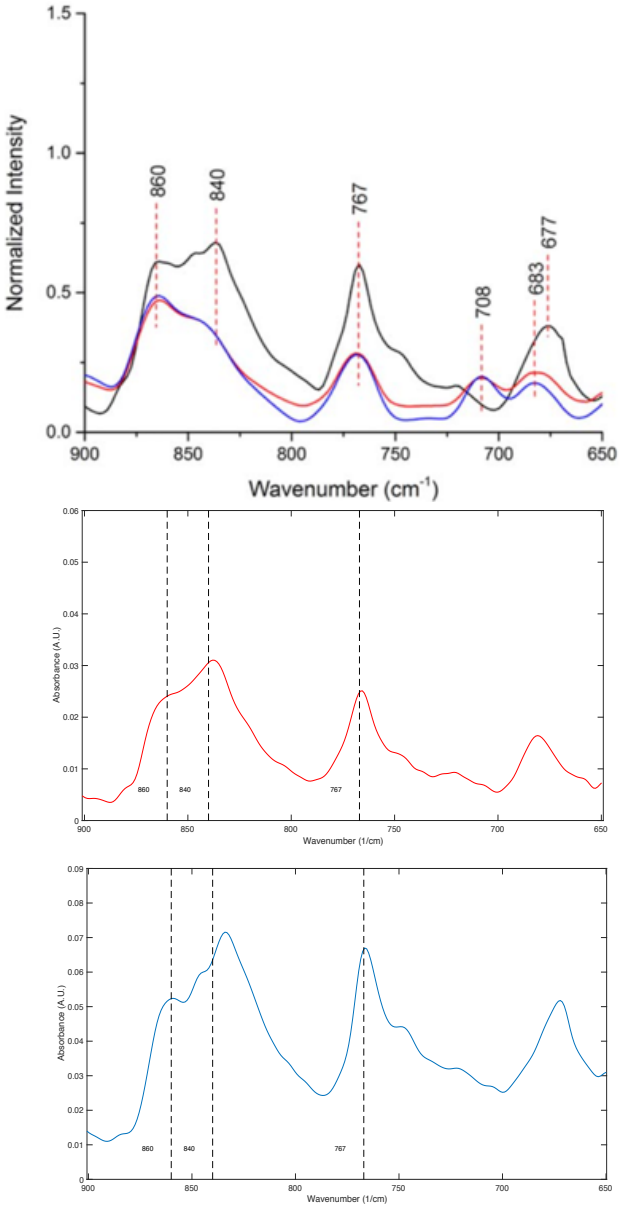

Figure 3.26: FTIR analyses of (top) PEEK and S-PEEK at two degrees of sulfontation, (middle) PEEK fibers, (bottom) native PEEK pellet. Note the diminished size of the 840 peak and the new peak at 708 in S-PEEK. This further shows a characteristic spectrum for S-PEEK that is distinct from PEEK. Top image from [11].

From an in-depth analysis of the FTIR spectra in Figures 3.24-3.26, the fibers produced in this thesis show a characteristic spectrum that aligns with literature values for native PEEK and is distinct from S-PEEK. However, small deviations between the PEEK

pellet and fiber suggest that they do not share the same crystalline morphology. Further testing with DSC and XRD will be necessary to fully explain these deviations.

3.5 – Optical Images

The final technique used to analyze the electrospun fibers was polarized optical microscopy (POM) with a Nikon Eclipse E600 POL microscope and a SPOT Insight CCD camera. A 32-micron diameter sample PEEK fiber was carefully removed from the aluminum foil collector and placed between two glass slides. The POM technique made it possible to illuminate the fiber with polarized light and then see the interaction between the polarized light and the molecules in the fiber. The fiber showed evidence of uniaxial birefringence [10]. When placed between two linear polarizers with their axes of polarization offset 90° from one another, the amount of light transmitted through the second polarizer, which will be referred to as the analyzer for clarity, depended on the rotational orientation of the fiber, as shown in Figure 3.25.

The wave of light passing through the microscope is an electric field wave travelling through space composed of two perpendicular component vectors, $\mathbf{E}_x$ and $\mathbf{E}_y$. The light from the microscope light source is natural light, and has no polarization state. However, once it passes through the polarizer, the light is linearly polarized, leaving just the $\mathbf{E}_x$ component travelling onwards to the fiber. If the fiber is in line with the analyzer, along the y-axis, then the light shows no change in polarization state and the transmitted light is cut out by the analyzer (Figure 3.27 image b). The analyzer removes any component of the light wave that is oscillating along the x-axis, so the original polarization state must have been unaltered as it passed through the fiber. Similarly, when the fiber is in line with the polarizer, along the y-axis, the light shows no change in polarization state and again the transmitted light is cut out by the analyzer (Figure 3.27 image f). However, at an angle of 45° to the polarizer, the

fiber clearly changes the polarization state of the light to allow a portion of it to pass through the analyzer. This means that some component of the light wave was oscillating along the y-axis after passing through the fiber. The reason for this is due to the uniaxial birefringence of the fiber. The $\mathbf{E}_x$ vector can be decomposed into two perpendicular component vectors in the x'-y' coordinate system shown in Figure 3.27 image d. Clearly, one component will oscillate in the y'-axis, along the fiber, and one component will oscillate in the x'-axis, perpendicular to the fiber. If the components travelled through the fiber at the same speed, then the polarization state of the light would not change as it left the fiber and, just as before, the analyzer would cut out the light. However, in this case not all the light is cut out, meaning that the index of refraction is not the same in all directions and one component is travelling faster than the other. This implies a shift in the relative amplitudes of the x' and y' components in time, meaning that the electric field no longer oscillates in just the x-axis, but has some amplitude in the y-axis when it leaves the fiber. Therefore, by changing the polarization state, the resulting amplitude along the y-axis is no longer zero and this component of the wave is passed through the analyzer to the camera.

This implies uniaxial birefringence within the fiber; the asymmetric polymer molecules in the fiber transmit light oscillating perpendicular to their length at a different speed than light oscillating parallel to their length. If there is large-scale parallel orientation of the molecules in the fiber, then the same behavior is seen in the fiber [13]. This is evident from this experiment, as the light wave component oscillating along the length of the fiber travels at a different speed than the light wave component oscillating perpendicular to the fiber. The results of this analysis do not indicate which is faster or slower, only that they are not identical. Therefore, the fiber shows large-scale molecular alignment either parallel or perpendicular to its length, represented by the y' and x' axes respectively. However, as stated in the previous section, related experiments with Nylon indicate polymer chain

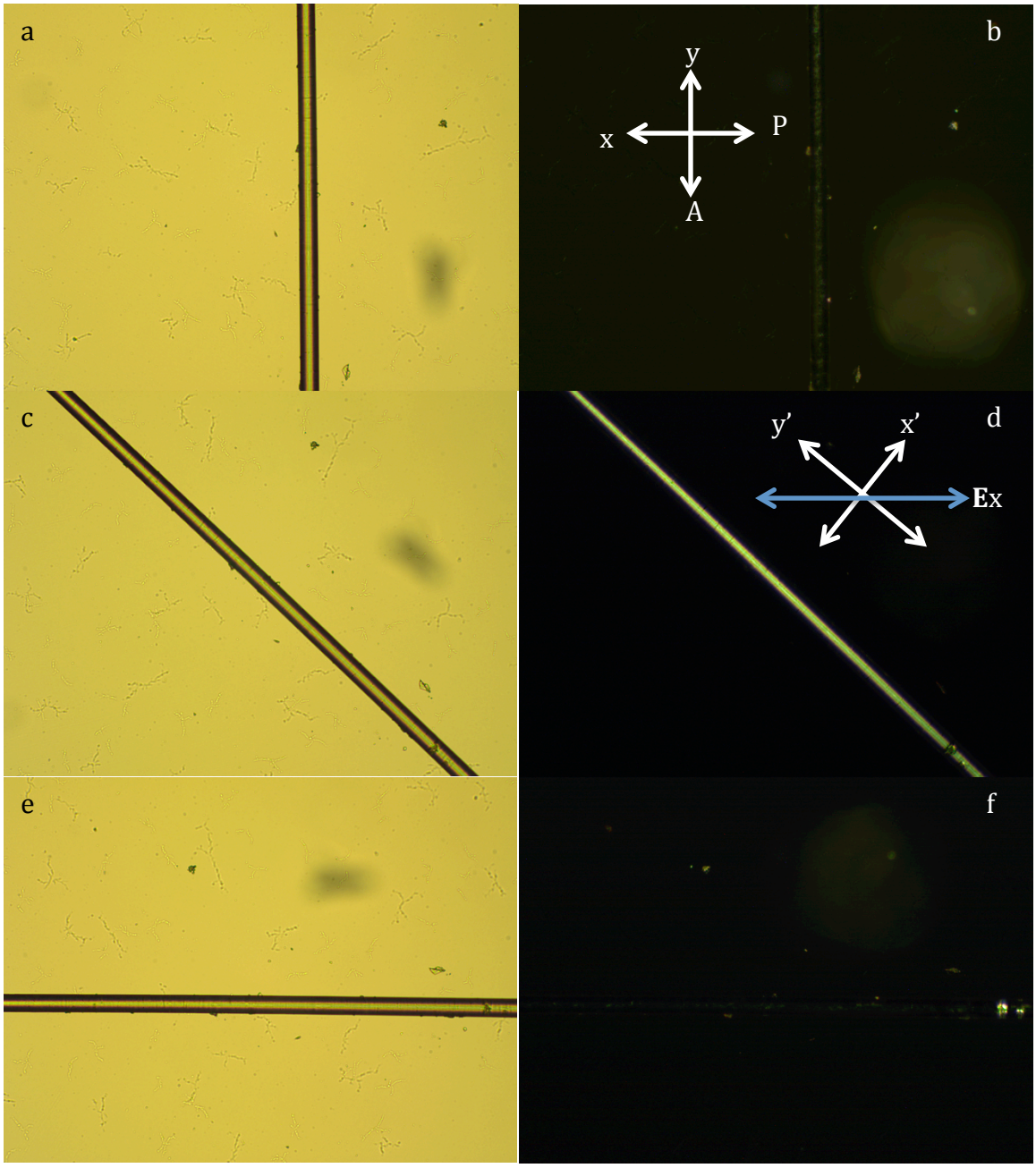

Figure 3.27: POM images of the 32-micron PEEK fiber under linearly polarized illumination at angles of 0, 45, and 90 degrees relative to the polarizer with no analyzer present (images a, c, e respectively). POM images of the same fiber at angles of 0, 45, and 90 degrees relative to the polarizer with the analyzer in place (images b, d, f respectively).

alignment along the axis of the fiber, parallel to its length [12]. Therefore, combining the birefringence of the fiber and this related evidence suggests that the electrospun PEEK

fibers show large-scale polymer chain alignment along the axial length of the fiber. Further testing will be required to determine which direction, parallel or perpendicular to the polymer chain, is the direction of the fast vibration for PEEK.

Chapter 3 References

[1] Li Z, Wang C. Chapter – 2, Effects of working parameters on electrospinning, 'One-Dimensional Nanostructures', Springer Briefs in Materials (2013), Pages 15-28. Doi: 10.1007/978-3-642-36427-3_2.

[2] Lee KH, Kim HY, Bang HJ, Jung YH, Lee SG. The change of bead morphology formed on electrospun polystyrene fibers, Polymer (2003), Volume 44, Issue 14, Pages 4029-4034. ISSN 0032-3861.

[3] Ribe N. Liquid rope coiling: A synoptic view, Journal of Fluid Mechanics (2017), Volume 812, Page 2. Doi: 10.1017/jfm.2016.836.

[4] Chiu-Webster S, Lister J. The fall of a viscous thread onto a moving surface: A 'fluid-mechanical sewing machine', Journal of Fluid Mechanics (2006), Volume 569, Pages 89-111. Doi: 10.1017/S0022112006002503.

[5] Brown T, Dalton P, Hutmacher D. Direct Writing By Way of Melt Electrospinning, Advanced Materials (2011), Volume 23, Issue 47, Pages 5651-5657. ISSN 1521-4095. Doi: 10.1002/adma.201103482.

[6] Callister WD, Rethwisch DG. 'Material Science and Engineering: an Introduction', Wiley (2017), 9th Edition, Pages 545- 629.

[7] Dalton P, Grafahrend D, Klinkhammer K, Klee D, Möller M. Electrospinning of polymer melts: phenomenological observations, Polymer (2007), Volume 28, Pages 6823–33. Doi: 10.1021/bm050777q.

[8] Patel P, Hull R, McCabe R, Flath D, Grasmeder J, Percy M. Mechanism of thermal decomposition of poly(ether ether ketone) (PEEK) from a review of decomposition studies, Polymer Degradation and Stability (2010), Volume 95, Issue 5, Pages 709-718. ISSN 0141-3910. Doi.: 10.1016/j.polymdegradstab.2010.01.024.

[9] Koziara BT, Kappert EJ, Ogieglo W, Nijmeijer K, Hempenius MA, Benes N. Thermal stability of sulfonated Poly(ether ether ketone) films: on the role of protodesulfonation, Macromolecular Materials and Engineering (2016), Volume 301, Pages 71–80. Doi: 10.1002/mame.201500075.

[10] Hecht E. 'Optics', Addison-Wesley (2017), 5th Edition, Pages 1-500.

[11] Sadrjahani M, Gharehaghaji AA, Javanbakht M. Aligned electrospun sulfonated polyetheretherketone nanofiber based proton exchange membranes for fuel cell applications, Polymer Engineering Science (2015), Volume 57, Pages 789–796. Doi: 10.1002/pen.24453.

[12] Zhmayev E, Cho D, Joo YL. Modeling of melt electrospinning for semi-crystalline polymers, Polymer (2010), Volume 51, Issue 1, Pages 274-290. ISSN 0032-3861. Doi: 10.1016/j.polymer.2009.11.025.

[13] Tagaya A, Koike Y. Compensation and Control of the Birefringence of Polymers for Photonics, Polymer Journal (2012), Volume 44, Issue 4, Pages 306-14.

Chapter 4 – Conclusions and Future Work

4.1- Experimental Limitations

Although the method presented in this thesis is clearly a successful technique for producing native PEEK fibers through melt electrospinning, there are several areas for improvement in future work.

The first area for improvement is in spinneret design. While the droplet of PEEK suspended on a wire tip was a simple and effective way to produce small amounts of PEEK fibers, it is impractical for the larger-scale manufacturing necessary for filters or textiles. For example, the droplet often fell off the wire tip during the spinning process, halting the spin. When the droplet did fall off, it often fell to the floor of the furnace or was sometimes drawn directly to the collector under high electric field strengths. In order for the production of PEEK fibers to be scaled up and the duration of spins to be increased, a high-temperature extruder must be designed and manufactured to allow for a constantly replenished supply of PEEK to form a droplet at the spinneret. Several methods can surely be envisioned for such a device, such as drilling a hole into the rear furnace wall so that the extruder mechanism could be placed outside the furnace and the PEEK pushed in to melt as it neared the spinneret (see Figure 4.1). However, the resulting need for precise control of temperature, flow rate, and destructively modifying the furnace were all beyond the scope of this thesis.

The second area for improvement is in temperature control of both the molten PEEK at the spinneret and the spin line. As stated in Sections 1.3, 2.2, and 3.2.3, the temperature gradient along the spin line has a significant effect on fiber morphology. Once up to temperature, the furnace used in this thesis was able to maintain the temperature

around the spinneret within plus or minus 5°C, as measured with a type K thermocouple before and after each spin.

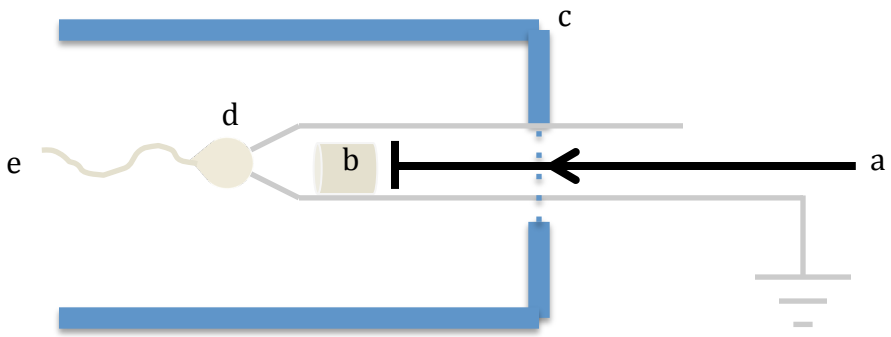

Figure 4.1: A possible spinneret design where a plunger applies a force (a) on PEEK pellets (b), while remaining outside the furnace (c) and forces them out of a grounded spinneret to form a droplet at a constant controlled rate (d). The fibers (e) can then be drawn to a high voltage collector.

However, the region of the spin line in the Macor door opening and on towards the collector had a far less stable temperature. In this region, the mixing of high temperature air with air at room temperature of about 21°C caused convection currents of turbulent air. This meant that a consistent temperature gradient along the spin line could not be guaranteed from one spin to another or even during the whole duration of one spin. To have better control over fiber morphology and eliminate uncontrolled working parameters, a method for controlling the spin line temperature gradient must be added to the method presented in this thesis.

A third improvement area is in the design of the collector. The collector used in this thesis was a stationary sheet of Aluminum foil at high voltage. However, one downside of this is that the PEEK fibers tended to congregate over a very small central area of the foil, (see Figure 4.2), similar to the behavior seen in Figure 3.19. Unlike the behavior seen in solution electrospinning by Renecker and Yarin [1], where the fluid jet gets whipped around

in the spin line and is distributed over a broad area of the collector (see Figure 4.3 for an example of PEO), the molten PEEK jet resulted in fibers all found within a 1 cm radius of the center of the collector. This was acceptable for most of the short time duration spins performed in this thesis, but for some spins where many fibers were deposited they would tend to bunch up into a mound rather than a more uniform flat distribution (see Figure 3.16 for this behavior becoming noticeable during a 5 minute spin). One simple remedy to this would be to employ a moving collector such as those outlined in Section 1.4. A moving collector, either rotating or translating in a plane, would be able to more evenly distribute the fibers over a broad area while still giving them a fairly random orientation, making it possible to form a large fiber mat more suited to real-world applications.

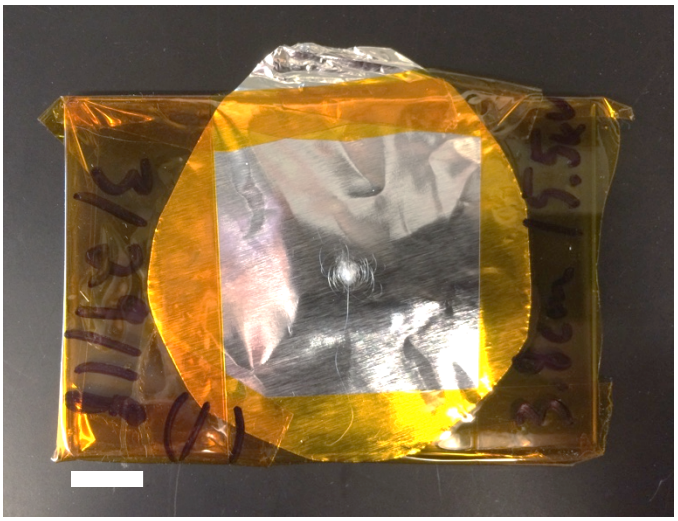

Figure 4.2: PEEK fibers from sample 10 on an Aluminum foil collector. Note the small distribution of fibers within a 1 cm radius, typical of this method. The scale bar is 1 cm.

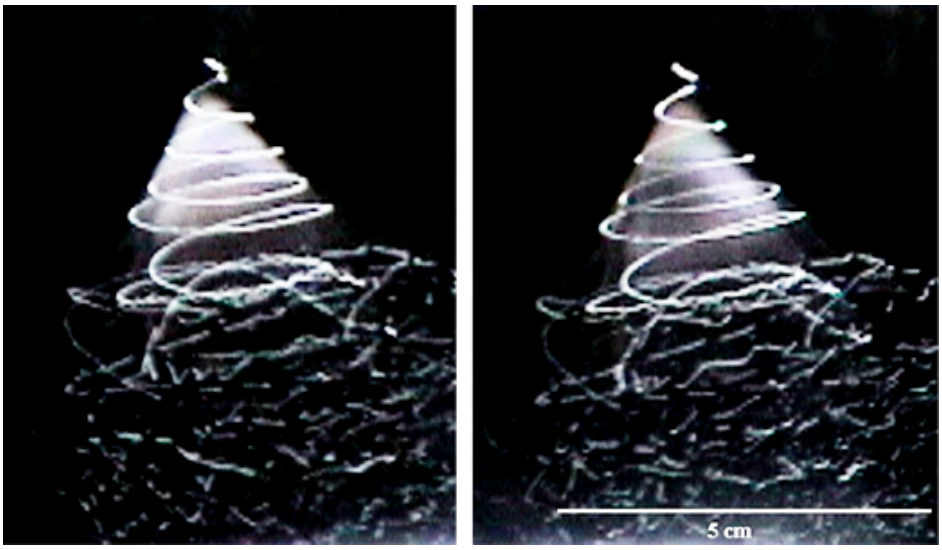

Figure 4.3: An electrospun jet of polyethylene oxide in the spin line, dissolved in a mixture of 75% water and 25% ethanol. Note the intense whipping and branching behavior that occurs as the jet travels down towards a grounded collector and expands into a large radius cone (Image from [1]).

A final area for improvement is in expanding the range of electric field strengths that can be used for electrospinning with this method. It was observed that arcing from the collector to the spinneret occurred at electric field strengths of roughly 4.9 kV/cm. Although this was sufficient for producing fibers for this thesis, it is possible that future research employing higher electric field strengths and spinneret designs could produce better fibers. As stated in Section 1.4, Equation 1.2 relates electrical breakdown in air to air temperature and pressure. By significantly increasing the air temperature within the furnace, the electrical breakdown voltage in this method was reduced to a level lower than at room temperature. This lowered the maximum voltage that could be applied to drive the electrospinning process. To counter this phenomenon, decreasing the ambient air pressure or using an ambient gas with a breakdown voltage higher than air would raise the breakdown voltage at high temperature. In either case, this would require placing the whole

spinning and heating apparatus within an airtight container. However, this level of construction was unnecessary to accomplish the goals of this thesis.

4.2 – Fiber Quality

The overall quality of the fibers produced in this thesis can be summarized in several ways. The resulting fiber mats were characterized by being made of one continuous fiber, forming a smooth cylindrical cross-section, and having a generally random orientation on the collector. There was also evidence of tapered beading, sudden decreases and increases in fiber diameter, as well as circular and figure-of-eight distributions in some cases. In general however, the method laid out in this thesis is a successful technique for producing PEEK fibers on the micron and sub-micron level in small quantities.

4.3 – Application Potential

First, as stated in Section 4.1, the fibers exhibited very little instability in the spin-line, as shown by their small distribution area on the collector. This is desirable for applications in direct writing (see Section 1.4), where the fiber needs to be placed precisely and accurately at the desired location. With the appropriate apparatus capable of slowly extruding the PEEK from a spinneret onto an x-y plane translatable collector, it seems reasonable to extrapolate that direct writing PEEK fibers is a possible application capable of producing PEEK fibers on the micron and possibly sub-micron level in an ordered way similar to 3-d printing. This could yield orientations such as linear rows, curved shapes, or any combination therein to form a woven mat for a number of applications including textiles and filtration [2]. However, as first stated in Section 3.2.3, the speed of such a translating collector will affect the alignment of molten fibers landing on its surface, and should be carefully set to achieve the desired orientation.

Second, this method has shown that PEEK fibers can be electrospun into mats of micron and sub-micron size fibers without the unwanted effects of sulfonation. Therefore, if the fiber diameter -and consequently the porosity- could be made more consistent, likely by the addition of a spinneret with controllable flow rate and nozzle size, it seems probable that an electrospun PEEK fiber mat could be applied to the types of filtration applications laid out in Section 1.4 such as chemical solvent, high temperature, or high stress filtration.

4.4 – Future Work

This thesis has shown the successful of production melt electrospun PEEK fibers, yet many new research questions can be envisioned for future work beyond the scope of this thesis. One possible area of research would be to observe and characterize the Taylor cone formation of PEEK from the simple wire spinneret used in this thesis. This behavior was impossible to observe using the apparatus in this thesis, as the spinneret was hidden behind the furnace door and collector, but future methods could allow for the Taylor cone to be directly observed. This could lend more insight into the unique fiber characteristics presented in Chapter 3.

Another area of future research would be to investigate ways to get more consistent PEEK fiber diameters under the same working conditions. This might require a new type of spinneret, a more controllable heat source, new combinations of working distance and applied voltage, or any other conceivable adaptation of the method presented in this thesis.

A final important area of future research is to investigate the crystal structure of melt electrospun PEEK fibers through methods such as X-Ray Diffration analysis and Differential Scanning Calorimetry. This would shed light onto the slight deviations in FTIR absorbance between the PEEK pellet and fiber, help explain the outlying occurrence of spherulites on the surface of one fiber, give a better understanding of the large-scale

polymer chain orientation suggested by birefringence, and would more completely detail the physical nature of these new and novel fibers.

In collaboration with the Cebe Polymer Physics Research Group at Tufts university, a project is planned for the Summer of 2018 to perform Differential Fast-Scanning Calorimetry on melt electrospun PEEK fibers spun onto copper Transmission Electron Microscopy grids. This research will hopefully be able to use very high heating rates of around 2,000 Kelvin per second to observe the heat flow in and out of the fibers without allowing enough time for reorganization of the crystals within the fibers [3]. This will give invaluable insight into the crystallization kinetics and structure of melt electrospun PEEK fibers.

Chapter 4 References

[1] Reneker DH, Yarin AL. Electrospinning jets and polymer nanofibers, Polymer (2008), Volume 49, Issue 10, Pages 2387-2425, ISSN 0032-3861,
Doi: 10.1016/j.polymer.2008.02.002.

[2] Dalton P, Vaquette C, Farrugia B, Dargaville T, Brown T, Hutmacher D. Electrospinning and additive manufacturing: converging technologies, Biomaterial Science (2013), Volume 1, Issue 2, Pages 171-185, The Royal Society of Chemistry. Doi: 10.1039/C2BM00039C

[3] Schawe J. Cooling rate dependence of the crystallinity at nonisothermal crystallization of polymers: A phenomenological model, Journal of Applied Polymer Science (2016), Volume 133, Issue 6, Pages 3-7. ISSN 1097-4628. Doi: 10.1002/app.42977